AD-A194 749 STUDIES OF COHERENT BEAM PROCESSING CONCEPTS PHASE 1 1/1
(U) ROCKWELL INTERNATIONAL THOUSAND OAKS CA SCIENCE
CENTER P A YEH ET AL MAR 88 SC5443.FR

UNCLASSIFIED N00014-85-C-0557 F/G 20/6 NL

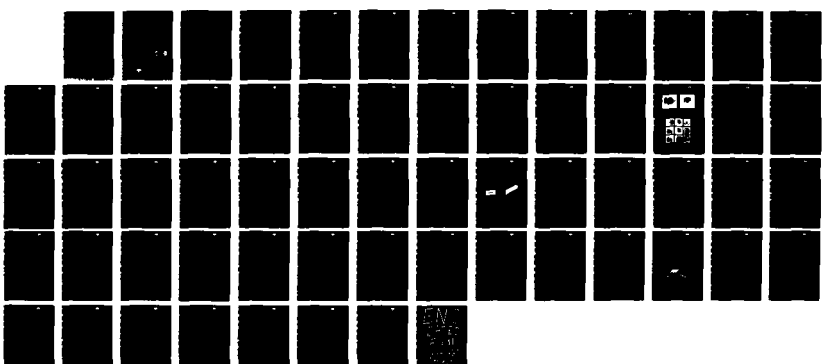


1.0
1.1
1.2
1.4
1.6
1.8
2.0
2.2
2.8
3.2
3.6
4.0
4.5
5.0

Copy No. 15

STUDIES OF COHERENT BEAM PROCESSING CONCEPTS

PHASE I FINAL REPORT FOR THE PERIOD September 1, 1985 through December 31, 1987

CONTRACT NO. N00014-85-C-0557

Prepared for

Office of Naval Research
800 N. Quincy Street
Arlington, VA 22217-5000

P.A. Yeh
Principal Investigator

MARCH 1988

Approved for public release; distribution unlimited

Rockwell International
Science Center

UNCLASSIFIED

SECURITY CLASSIFICATION OF THIS PAGE

REPORT DOCUMENTATION PAGE

FORM APPROVED
OMB No. 0704-0188

1a REPORT SECURITY CLASSIFICATION
UNCLASSIFIED

1b. RESTRICTIVE MARKINGS

2a. SECURITY CLASSIFICATION AUTHORITY

2b. CLASSIFICATION/DOWNGRADING SCHEDULE

3. DISTRIBUTION/AVAILABILITY OF REPORT
Approved for public release; distribution unlimited

4. PERFORMING ORGANIZATION REPORT NUMBER(S)
SC5443.FR

5. MONITORING ORGANIZATION REPORT NUMBER(S)

6a. NAME OF PERFORMING ORGANIZATION
ROCKWELL INTERNATIONAL Science Center

6b. OFFICE SYMBOL (If Applicable)

7a. NAME OF MONITORING ORGANIZATION

6c. ADDRESS (City, State, and ZIP Code)
1049 Camino Dos Rios Thousand Oaks, CA 91360

7b. ADDRESS (City, State and ZIP Code)

8a. NAME OF FUNDING/SPONSORING ORGANIZATION
Office of Naval Research

8b. OFFICE SYMBOL (If Applicable)

9. PROCUREMENT INSTRUMENT IDENTIFICATION NUMBER
CONTRACT NO. N00014-85-C-0557

8c. ADDRESS (City, State and ZIP Code)
800 North Quincy Street Arlington, VA 22217-5000

10. SOURCE OF FUNDING NOS.

PROGRAM ELEMENT NO	PROJECT NO	TASK NO	WORK UNIT ACCESSION NO

11. TITLE (Include Security Classification)
STUDIES OF COHERENT BEAM PROCESSING CONCEPTS

12. PERSONAL AUTHOR(S)
Yeh, Pochi A., Chiou, Arthur E.T., McMichael, Ian C., Khoshnevisan, Monte

13a. TYPE OF REPORT	13b. TIME COVERED	14. DATE OF REPORT (Year, Month, Day)	15. PAGE COUNT
Phase I Final Report	FROM **09/01/85** TO **12/31/87**	**1988, MARCH**	**59**

16. SUPPLEMENTARY NOTATION

17. COSATI CODES			18. SUBJECT TERMS (Continue on reverse if necessary and identify by block number)
FIELD	GROUP	SUB-GROUP	

19. ABSTRACT (Continue on reverse if necessary and identify by block number)

We report the results of theoretical and experimental studies to investigate nonlinear optical (NLO) two-wave mixing phenomena for coherent beam processing. Steady state energy exchange via two-wave mixing occurs naturally in photorefractive crystals in response to laser beams. Such energy exchange is nonreciprocal and can lead to large transfer of energy from one beam to another. However, we have shown that there is no crosstalk between either the temporal or spatial phases of the two beams, i.e., only optical energy and not the phases is transferred. Thus a weak signal beam with a planar wavefront can be greatly amplified with high fidelity at the expense of a strong pump beam with an aberrated wavefront. We have also shown that two-wave mixing can be generalized to materials other than photorefractive crystals. This project was concerned with studying the physics and applications of generalized photorefractive two-wave mixing for laser beam processing (e.g., cleanup, steering, or combining).

20. DISTRIBUTION/AVAILABILITY OF ABSTRACT
UNCLASSIFIED/UNLIMITED ☐ SAME AS RPT ☒ DTIC USERS ☐

21. ABSTRACT SECURITY CLASSIFICATION
UNCLASSIFIED

22a. NAME OF RESPONSIBLE INDIVIDUAL
Lt. Kenneth P. Morton

22b. TELEPHONE NUMBER (Include Area Code)

22c. OFFICE SYMBOL

DD FORM 1473, JUN 86 **Previous editions are obsolete.**

UNCLASSIFIED

SECURITY CLASSIFICATION OF THIS PAGE

We have studied two-wave mixing in photorefractive media for laser beam cleanup and combining. We have also developed and demonstrated a scheme for using a combination of two-wave mixing and optical phase conjugation to overcome any aberrations which may be present in the nonlinear crystals. In addition, we studied how the general principles of photorefractive energy exchange may be extended to higher power regime, beyond those tolerable by photorefractive crystals. It was established that the nonlocal response of photorefractive media, which produces the nonreciprocal energy exchange can be "mimicked" in other types of nonlinear media which are not photorefractive. This allows the extension of the concept to "artificial" photorefractive media which can tolerate higher optical powers, and can have much faster response times. It was shown that the equations governing the artificial photorefractive effects, i.e., two-wave mixing in Kerr media, are indeed quite analogous to two-wave mixing in photorefractive crystals. It was also shown that artificial photorefractive effects are also inclusive of other well-known stimulated scattering effects such as Stimulated Brillouin Scattering (SBS), when initiated by an injection process.

Our studies of two-wave mixing in Kerr media concentrated on electrostrictive nonlinearities. General relationships were discovered which yielded information on electrostrictive Kerr nonlinearities of materials, simply from their linear acousto-optical parameters. In addition, we discovered the Kerr-Bragg effect, a process by which a weak acoustically generated optical seed beam in a nonlinear Kerr medium can become very strong by NLO two-wave mixing effects. It was found that the Kerr-Bragg effect can be potentially used for agile steering of high energy laser beams, because at high optical energies, essentially all of the optical energy from the input beam would be transferred to the weak acousto-optically generated seed beam. Analytical expressions were developed which model the Kerr-Bragg process, and proof-of-concept experiments were carried out. Applications studies for the Kerr-Bragg process, as well as generalized nondegenerate two-wave mixing were also carried out and future demonstration experiments were examined. In addition to cleanup and agile beam steering, it was found that our general concepts have potential applications for laser beam combining, phase locking of laser arrays and laser beam phase control.

FOREWORD

The effort described in this report was a basic science study to examine innovative nonlinear optical concepts for control of coherent light. Funding support was from the Innovative Science and Technology Office of the Strategic Defense Initiative (SDI/ISTO), and monitored through an Office of Naval Research grant, Contract No. N00014-85-C-0557. Technical contributors to this phase of the program were the following:

Dr. Pochi Yeh (theory, Principal Investigator)
Dr. Monte Khoshnevisan (modeling, high power laser experiments)
Dr. Arthur Chiou (experiments in photorefractive media)
Dr. Ian McMichael (Kerr-Bragg demonstration experiments)

The authors would like to gratefully acknowledge helpful discussions with Dr. Matthew B. White (ONR/SDIO/ISTO), and Lt. Kenneth P. Morton, our ONR Contract Monitor. Helpful contributions from Dr. Tai Chi Wang and Dr. Tallis Chang at the Science Center are also gratefully acknowledged.

TABLE OF CONTENTS

LIST OF FIGURES

LIST OF FIGURES

LIST OF TABLES

1.0 INTRODUCTION

Energy exchange phenomena in nonlinear optics are of considerable interest for coherent processing of laser beams. For example, steady state (and nonreciprocal) energy transfer between coherent beams in photorefractive crystals is finding a great deal of potential applications employing low power laser beams. These applications include image amplification,[1] vibrational analysis,[2] self-oscillation,[3-5] nonlinear optical laser radar receiver,[6] wavelength agile rejection filters for laser hardening,[7] and many types of self-pumped phase conjugators, and optically nonreciprocal processes[8] which operate on the basis of two-wave mixing gain in photorefractive media. Two-wave mixing effects can also be used for laser beam cleanup or combining,[9] although photorefractive materials can not be used to perform such processing at high laser powers.

Several unique beam processing concepts have been generated at the Rockwell International Science Center which utilize the nonreciprocal energy transfer and the lack of phase crosstalk[9] in photorefractive two-wave mixing. The process normally requires electro-optic (noncentrosymmetric) crystals. Our studies within this program have focused on investigations of coherent beam processing in photorefractive media, and extensions of the concept to what we refer to as "artificial" photorefractive effect, in order to allow two-wave mixing in media that are normally not photorefractive. We predicted that such artificial two-wave mixing can be induced in centrosymmetric media, a phenomenon which is (in steady state) forbidden by symmetry. A particular advantage of a number of such media is that they are much faster, and can tolerate considerably higher optical powers than the photorefractives.

Our studies in this program have resulted in a number of interesting findings (see Sect. 2). In addition to the experiments carried out in photorefractive crystals, we studied two-wave mixing in (centrosymmetric) Kerr media via electrostrictive nonlinearities. A phenomenon of particular interest to this proposal was discovered, a nonlinear process called "Kerr-Bragg scattering."[10] This effect was predicted, theoretically analyzed, and recently demonstrated. Predictions were for steady state energy exchange which is artificially induced in an electrostrictive Kerr medium by phase matching nondegenerate two-wave mixing holograms to certain acoustic waves in the medium. This effect is of interest to Strategic Defense Initiative (SDI) because the process has a threshold and is expected to improve greatly as the laser power or energy is increased. One immediate

application foreseen for the Kerr-Bragg process was for agile steering of high energy laser beams. Injection of weak acoustic beams triggers the nonlinear Kerr mixing and the high power beam quickly switches in the direction of its Bragg diffraction from the acoustic seed beam. Fast and randomly selectable deflection of a primary high power beam thus becomes possible with high numbers of resolvable spots in the direction of single or possibly multiple targets.

Our findings constitute the beginnings of the field of nonlinear acousto-optics, where small acoustic fields are used to trigger large nonlinear optical events for applications in agile beam steering. The same concept has ramifications for laser beam combining, phase locking of laser arrays, and laser beam phase control. For example, alternate configurations are possible for injecting the (frequency downshifted) optical seed beam separately, instead of producing it in the nonlinear medium by the seed acoustic beam. Then resonant nondegenerate two-wave mixing will itself generate the seed acoustic beam, and further amplify it by the Kerr-Bragg effect. The advantage of this process over the original Kerr-Bragg effect is that the acoustic beam profile is expected to be more uniform in the medium, particularly for high acoustic frequencies. Moreover, this process is more applicable to short optical pulses ($\leq$ 1 μs). There are, however, some drawbacks related to more stringent requirements for angular matching, and potentially higher optical energy thresholds, as compared with the Kerr-Bragg process.

This report summarizes the results of our Phase I effort. In a proposed continuation effort, we aim to carry out further studies on the Kerr-Bragg process, resonant nondegenerate two-wave mixing effects, and related phenomena, and apply them to developing agile beam steering devices for SDI applications.

2.0 PROGRESS

2.1 Progress Summary

Our original objectives in the program were to carry out basic research on nonlinear optical methods for coherent beam processing. We have made significant progress in a number of areas. These include theoretical modeling, experiments on photorefractive crystals to study the physics of beam cleanup and combining via two-wave mixing energy exchange, discovery of the Kerr-Bragg effect, as well as modeling of the Kerr-Bragg and related processes and experiments to demonstrate the effect. The highlights are listed below:

* Theoretical modeling of two-wave mixing in Kerr media

* Demonstration of beam cleanup and combining in photorefractive crystals, identification of problems

* Photorefractive two-wave mixing and aberration correction by phase conjugation

* Determination of relationships between nonlinear electrostrictive Kerr effect and acousto-optic properties of materials

* Discovery of the Kerr-Bragg (K-B) Effect, theoretical modeling of the K-B process, numerous experiments, determination of the requirements, recent demonstration of the effect.

More details of this progress are presented later in this report. Aside from a great deal of scientific findings, the Kerr-Bragg process and other artificial photorefractive effects such as nondegenerate two-wave mixing in Kerr media studied here may indeed have applications for agile beam steering, or phase locking of high energy lasers. A list of publications/presentations based on our effort is given in Table 2.1.

Table 2-1

List of Program Publications/Presentations

1. "Laser Beam Cleanup by Mode Filtering and Photorefractive Two-wave Mixing," A.E.T. Chiou, P. Yeh, M. Khoshnevisan, Paper ThM2 CLEO '86, San Francisco, CA (June 1986).

2 "Laser Beam Cleanup Using Photorefractive Two-wave Mixing and Optical Phase Conjugation," A.E.T. Chiou, P. Yeh, Opt. Lett. 11, 461 (1986).

3. "Exact Solution of a Nonlinear Model of Two-Wave Mixing in Kerr Media," P. Yeh, JOSA (B), B-3, 747 (1986).

4. "Kerr-Bragg Agile Beam Steering Device," M. Khoshnevisan, P. Yeh, Science Center Patent Disclosure, Docket #86SC3 (1986).

5. "Two-Wave Mixing for Coherent Beam Processing," P. Yeh, A.E.T. Chiou, M. Khoshnevisan, SDIO/DEO Workshop on Nonlinear Optical Techniques for SDI Applications, Kirtland AFB, NM (October 1986).

6. "Coherent Beam Processing," M. Khoshnevisan, A.E.T. Chiou and P. Yeh, Quantum Electronics Conference, Snowbird, Utah (1987).

7. "Relationship Between Nonlinear Electrostrictive Kerr Effects and Acousto-optics," M. Khoshnevisan and P. Yeh, presented at SPIE, O-E LASE '87, Los Angeles, CA (January 1987). (Invited paper) SPIE Proc. 739, 82 (1987).

8. "Nonlinear Optical Bragg Scattering in Kerr Media," P. Yeh and M. Khoshnevisan, JOSA (B) 4, 1954 (1987).

9. "Laser Beam Processing Concepts," P. Yeh, A.E.T. Chiou, I. McMichael and M. Khoshnevisan, presented at SPIE O-E LASE '88 (Space Power and Directed Energy Program), Jan. 1988, Los Angeles, CA.

10. "Nonlinear Optical Bragg Scattering in an Electrostrictive Kerr Medium," I. McMichael, M. Khoshnevisan, P. Yeh, in preparation for submittal to Optics Letter, 1988.

2.2 Progress Details

We present a brief account of the progress in the Phase I of the project in the following subsections.

2.2.1 Modeling of Two-Wave Mixing in Kerr Media

The coupling of two electromagnetic waves in Kerr media was considered, and an exact solution of the coupled-mode equations was derived in the most general case when both the pump depletion and material absorption were considered. This theory is the foundation of the process that we call "artificial" photorefractive effect. It describes how the local holographic response of the Kerr media (i.e., holograms in phase with the optical interference pattern that produces them) can be modified to produce nonlocal nonlinearities. The method considered to produce this modification is via a frequency shift between the two beams, or nondegenerate two-wave mixing. Due to the finite response time of the Kerr medium, a spatial phase shift is thus induced between the interference patterns and the nonlinear holograms produced in the medium. This phase shift is analogous to that which occurs naturally in photorefractive media, and allows steady state nonreciprocal energy exchange between the beams.

2.2.1.1 Exact Solution of a Nonlinear Model of Two-Wave Mixing in Kerr Media

The propagation of electromagnetic waves in media possessing a strong Kerr effect is one of long and sustained interest.[11,12] A number of various phenomena manifest themselves at high incident beam powers. This includes self-phase modulation,[13] mode-locking[14] and self-focusing.[15-18] The effect is described by a dependence of the index of refraction on the electric field according to

$$n = n_0 + n_2 \langle E^2 \rangle \qquad (1)$$

where $\langle E^2 \rangle$ is the time average of the varying electric field.

In the analysis that follows, we consider the case of codirectional two-wave mixing in a Kerr medium. The two waves form an interference pattern which corresponds to a spatially periodic variation of the time-averaged field $\langle E^2 \rangle$. In a Kerr medium, such a periodic intensity produces a volume grating. Thus, the problem we address is most closely

related to the phenomenon of self-diffraction from an induced grating. The formulation of such a problem is very similar to that of the holographic two-wave coupling in photorefractive crystals.[19-21] However, there exists a fundamental difference between these two types of two-wave mixing. In photorefractive media, the index modulation is proportional to the contrast of the interference fringes, whereas in Kerr media, the index modulation is directly proportional to the field strength. Thus, in Kerr media, the coupling strength is proportional to the beam intensities, where in photorefractive media, the coupling strength is determined by the ratio of beam intensities.[8,22,23]

In this section, we solve the coupled equations for the codirectional coupling and obtain exact solutions for the amplitude of the two waves. Let the electric field of the two waves be written

$$E_j = A_j \exp[i(\omega_j t - \vec{k}_j \cdot \hat{r})] \qquad j = 1,2 \tag{2}$$

where ω_j's are the frequencies and $\vec{k}_j$'s are the wave vectors. In Eq. (2) we assume for simplicity that both waves are s-polarized and the medium is isotropic. We further assume that no optical rotation is present in the material. A_1 and A_2 are the amplitudes and are taken as functions of z only for a steady-state situation. The z-axis is taken normal to the surface of the medium (see Fig. 1).

SC85-32728

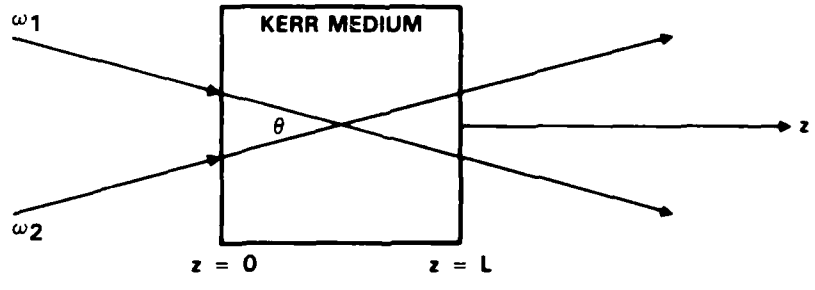

Fig. 1 Schematic diagram of two-wave mixing in Kerr media.

In the Kerr medium (from z = o to z = ℓ), these two waves generate an interference pattern. Such a pattern is traveling if $\omega_1 \neq \omega_2$. This interference pattern is described by $\langle E^2 \rangle$, where E is the total electric field

$$E = E_1 + E_2 \tag{3}$$

and the averaging is taken over a time interval T such that

$$\omega_{1,2} T >> 1 \tag{4}$$

and

$$|\omega_2 - \omega_1| T << 1 \quad . \tag{5}$$

Using $\langle E^2 \rangle = 1/2\ \mathrm{Re}[E^* E]$ and Eqs. (2) and (3), we obtain[24]

$$\langle E^2 \rangle = \frac{1}{2} \{ |A_1|^2 + |A_2|^2 + A_1^* A_2\, e^{i(\Omega t - \vec{K}\cdot\vec{r})} + A_1 A_2 I\, e^{-i(\Omega t - \vec{K}\cdot\vec{r})} \} \tag{6}$$

where

$$\Omega = \omega_2 - \omega_1 \tag{7}$$

and

$$\vec{K} = \vec{k}_2 - \vec{k}_1 \quad . \tag{8}$$

This interference pattern (6) induces an index volume grating via the Kerr effect. In general, the index grating will have a finite phase shift relative to the interference pattern because of the time-varying nature of the pattern. Thus, we can generalize Eq. (1) and write the fundamental components of Kerr-induced grating as

$$n = n_0 + \Delta n_0 + \frac{1}{2} \{ n_2\, e^{i\phi}\, A_1^* A_2\, e^{i(\Omega t - \vec{K}\cdot\vec{r})} + \text{c.c.} \} \tag{9}$$

where both ϕ and n_2 are real, and Δn_0 is a uniform change in index. Here, again, for the sake of simplicity, we assume a scalar grating. The phase ϕ indicates the degree to which the index grating is temporally delayed (or spatially shifted) with respect to the interference pattern. Generally speaking, both n_2 and ϕ are functions of Ω.[1,25]

Now, by using Eq. (9) for n and the scalar wave equation and by using the parabolic approximation (i.e., slowly varying amplitudes), we can derive the following coupled equations:

$$\frac{d}{dz} A_1 = -i \frac{\omega^2 n_o n_2}{2 k_z c^2} e^{-i\phi} |A_2|^2 A_1$$

$$\frac{d}{dz} A_2 = -i \frac{\omega^2 n_o n_2}{2 k_z c^2} e^{i\phi} |A_1|^2 A_2 \qquad (10)$$

where we assume that $\omega_2 \simeq \omega_1 = \omega$ and k_z is the z-component of the wave vectors [i.e., $k_z = k_1 \cos (1/2)\,\theta \simeq k_2 \cos (1/2)\,\theta$]. The parameter θ is the angle between the two beams. In Eq. (10), we have neglected the term Δn_o.

We now write

$$A_1 = \sqrt{I_1}\, e^{i\psi_1}, \quad A_2 = \sqrt{I_2}\, e^{i\psi_2} \qquad (11)$$

where ψ_1 and ψ_2 are the phases of the amplitudes A_1 and A_2, respectively. Using Eqs. (10) and (11), the coupled equations (10) can be written as

$$\frac{d}{dz} I_1 = -gI_1I_2 - \alpha I_1$$

$$\frac{d}{dz} I_2 = gI_1I_2 - \alpha I_2 \qquad (12)$$

and

$$\frac{d}{dz} \psi_1 = -\beta I_2$$

$$\frac{d}{dz} \psi_2 = -\beta I_1 \qquad (13)$$

where

$$g = \frac{2\pi}{\lambda \cos (\theta/2)} n_2 \sin \phi \qquad (14)$$

$$\beta = \frac{\pi}{\lambda \cos (\theta/2)} n_2 \cos \phi \quad . \qquad (15)$$

In Eqs. (12), we have added the attenuation term due to bulk absorption. The parameter α is the absorption coefficient. Note that beam 2 will be amplified, provided $gI_1 > \alpha$, according to Eq. (12).

The coupled equations (12) can be integrated exactly, and the solution is (see Appendix A)

$$I_1(z) = I_1(o) \cdot \frac{1 + m^{-1}}{1 + m^{-1} \exp[\frac{\gamma}{\alpha}(1 - e^{-\alpha z})]} \cdot e^{-\alpha z} \tag{16}$$

$$I_2(z) = I_2(o) \cdot \frac{1 + m}{1 + m \exp[-\frac{\gamma}{\alpha}(1 - e^{-\alpha z})]} \cdot e^{-\alpha z} \tag{17}$$

where m is the input beam ratio and is given by

$$m = \frac{I_1(o)}{I_2(o)} \quad , \tag{18}$$

and γ is given by

$$\gamma = g[I_1(o) + I_2(o)] \quad . \tag{19}$$

Substituting Eqs. (16) and (17) for I_1 and I_2, respectively, into Eqs. (13) and carrying out the integrations, we obtain

$$\psi_1(z) - \psi_1(o) = \frac{\beta}{g} \log \{\frac{1 + m^{-1}}{1 + m^{-1} \exp[\frac{\gamma}{\alpha}(1 - e^{-\alpha z})]}\} \tag{20}$$

and

$$\psi_2(z) - \psi_z(o) = -\frac{\beta}{g} \log \{\frac{1 + m}{1 + m \exp[-\frac{\gamma}{\alpha}(1 - e^{-\alpha z})]}\} \quad . \tag{21}$$

If we can neglect absorption (i.e., $\alpha = o$), then $I_2(z)$ is an increasing function of z and $I_1(z)$ is a decreasing function of z, according to Eqs. (16) and (17), provided γ is positive. Transmittance for both waves, for the lossless case, according to Eqs. (16) and (17), are

$$T_1 \equiv \frac{I_1(\ell)}{I_1(o)} = \frac{1 + m^{-1}}{1 + m^{-1} \exp(\gamma \ell)} \quad , \tag{22}$$

$$T_2 = \frac{I_2(\ell)}{I_2(o)} = \frac{1 + m}{1 + m \exp(-\gamma \ell)} \tag{23}$$

where m is the incident intensity ratio $m = I_1(o)/I_2(o)$. Note that $T_2 > 1$ and $T_1 < 1$ for positive γ. The sign of γ is determined by the sign of n_2 and the phase shift ϕ. Interestingly, these expressions are formally identical to those of the photorefractive coupling. The major difference is that the γ for Kerr media is proportional to the total power density of the waves, according to Eq. (19).

Figure 2 illustrates the intensity variation with respect to z for the case when g = 10 cm/MW, $\alpha = 0.1\ cm^{-1}$, $I_1(o) = 100\ KW/cm^2$, and $I_2(o) = 1\ KW/cm^2$. Note that even with the presence of absorption, the intensity of beam 2 increases as a function of z until $z = \ell_c$ where the gain equals the loss. Beyond $z = \ell_c$, the intensities of both beams are decreasing functions of z.

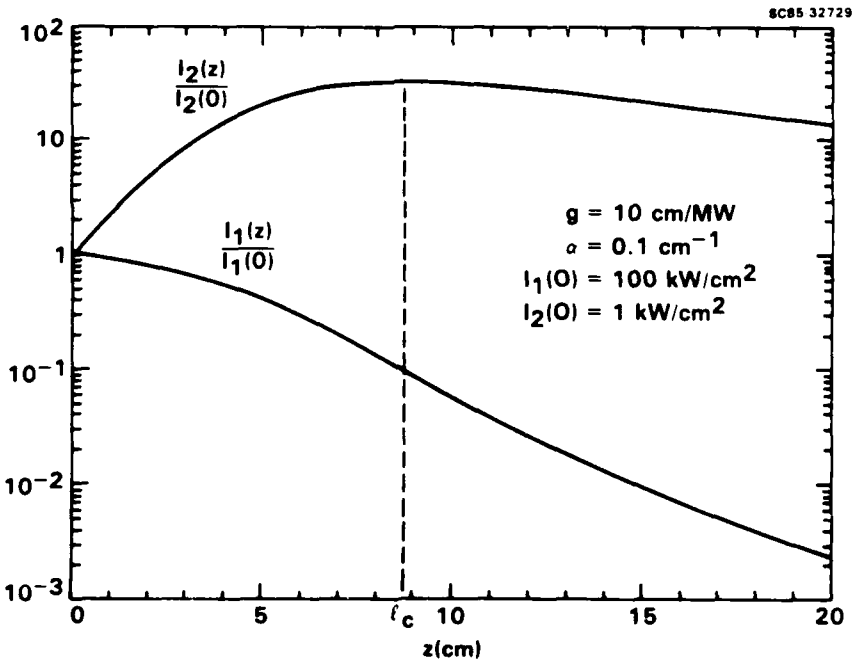

Fig. 2 Intensity variation with respect to z in the Kerr medium.

To summarize this section, we have derived the solution for the intensities, as well as the relative phase shift, for the codirectional two-wave mixing in Kerr media. Expressions for the beam intensities are obtained. They are shown to be formally identical to those of the holographic two-wave mixing in photorefractive crystals. The nonreciprocal energy transfer of the coupling may be used in various optical applications.

2.2.2 Two-Wave Mixing Experiments in Photorefractive Crystals

We carried out a number of experiments in photorefractive crystals, in order to test the general theoretical expectations for energy exchange without spatial or temporal crosstalk. The motivation for these experiments was to examine beam cleanup and beam combining. It was recognized that photorefractive materials would be unsuitable for eventual SDI applications of beam processing. However, these measurements were also recognized to be excellent and cost effective ways of testing the coherent beam processing theories at low optical powers. The relevance of such studies was established based on the considerable similarities that we uncovered between the equations governing energy exchange in photorefractive media and artificial photorefractive effects (nondegenerate two-wave mixing) in Kerr media.

2.2.2.1 Beam Cleanup by Photorefractive Two-Wave Mixing

Figure 3 shows the general concept proposed for cleaning up a multi-mode or aberrated laser beam by using photorefractive energy exchange. A part of the input beam is split off, and perhaps spatially filtered (not shown in the figure), and used as a seed beam in the two-wave mixing process in a photorefractive medium. This will approximate a gaussian TEM_{00} mode as the seed beam. All of the remaining parts of the input beam are then used as the pump beam(s), transferring their energy to the seed beam in the photorefractive medium. The result is expected to be a clean TEM_{00} mode beam, considerably amplified at the expense of the side lobes. Our experiments were carried out in crystals of $BaTiO_3$ and strontium barium niobate (SBN).

The results of our experiments (published in the Digest of Ref. 1, Table 2.1) can be summarized as follows: The energy exchange process produces significant gains (e.g., 10-100, or more) for the seed beam, which will carry off major portions of the overall input beam. The conditions, however, are that the beam overlap configurations in the nonlinear medium must be arranged carefully to ensure uniform energy transfer across the beam front of the seed beam. Moreover, the side lobes have to have nearly the same frequency as the seed beams, to within the photorefractive bandwidth of medium. For low to medium intensities, this bandwidth is very narrow for photorefractive crystals. Since the side lobes of many laser beams are significantly frequency shifted with respect to the central lobe, complete cleanup of laser beams requires faster photorefractive crystals, or artificially

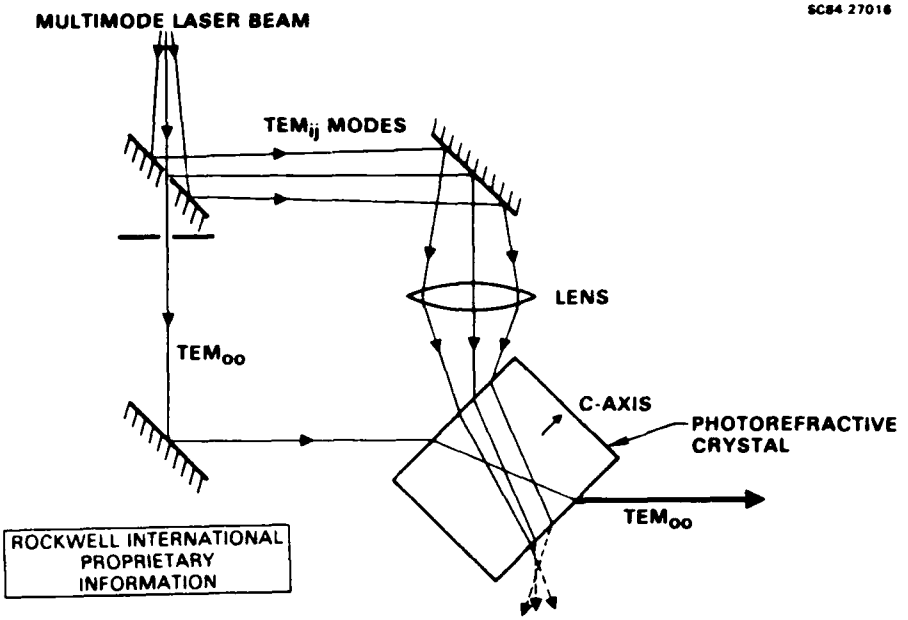

Fig. 3 Conceptual drawing of a laser beam cleanup experiment using photorefractive two-wave mixing.

induced photorefractive effects. The photorefractive process, however, can be used to correct aberrations in the laser beams, or to combine the beams of phase locked (but not with identical phases) lasers. The artificial photorefractive effects in fast Kerr media would be more promising for laser beam cleanup, where the frequency differences between the seed and the pump beams from the side lobes would be tolerable.

2.2.2.2 Beam Cleanup Using Photorefractive Two-Wave Mixing and Phase Conjugation

Our beam cleanup experiments pointed to a potential problem if the photorefractive (or artificially photorefractive) medium has inhomogeneities or aberrations. These aberrations will then be imprinted on the amplified and cleaned up seed beam. We conceived of and demonstrated a new concept (published in Ref. 2, Table 2.1) for correcting such aberrations using a phase conjugation process in conjunction with the two-wave mixing process.

An interesting note is that a similar concept has been independently pursued and recently demonstrated through some elegant (and considerably more costly) experiments at Naval Research Laboratory (Ref. 26) using high energy lasers. The results, of course, are similar to ours. As mentioned earlier, the photorefractive processes do indeed behave similar to the stimulated processes that occur at high laser powers.

The technique of using a phase-aberrated pump beam to amplify a clean seed beam by nonlinear optical processes such as photorefractive two-wave mixing[9,27] and stimulated Raman scattering[28-30] has been investigated for applications in laser beam cleanup. In all cases, the seed beam gains energy from the pump, and yet the phase aberration of the pump beam is not transferred to the seed beam. In general, however, both the pump and the seed beams are subjected to phase aberration caused by the gain medium itself, and the amplified output will bear the signature of the seed aberration. Recently, we reported the cleanup of the spatial and temporal phase aberration of a laser beam using photorefractive two-wave mixing in a strontium barium niobate (SBN) crystal.[9,27] In this section, we report the results of an experimental investigation on wavefront distortion of the beams due to imperfections (surface and bulk) of the photorefractive crystal. We also demonstrate a scheme in which phase conjugation eliminates such distortion.

The problem of two-wave mixing in photorefractive media has been formulated and solved by many workers,[8,19-22] and the basic properties relevant to beam cleanup are discussed by the authors.[9,27] In this section a new scheme is described that combines the advantages of photorefractive gain and the optical phase conjugation to achieve high fidelity in laser beam cleanup. Schematic diagrams illustrating the basic geometry of two-wave mixing without and with phase conjugation are shown in Fig. 4a and 4b, respectively. Note that in the latter the pumped beam is redirected to amplify the phase-conjugated signal beam (ρE^*_{st}) instead of the incident seed beam (E_S). A similar idea was pursued by Chang et al[31] for reduction of aberration in simulated Raman scattering.

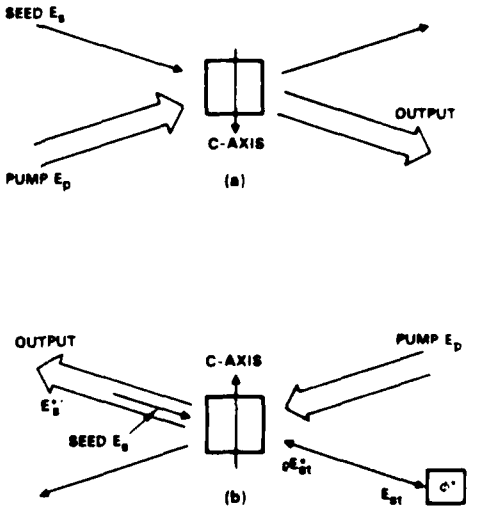

Fig. 4

Schematic illustrating the basic geometry for (a) two-wave mixing without phase conjugation, and (b) two-wave mixing with phase conjugation.

When a phase aberrator is introduced so that it intercepts only the pump beam, both schemes give a good quality output, and the phase conjugation of the incoming seed beam, as shown in Fig. 4b, is unnecessary. However, when the phase aberrators intercept both the pump and the seed beams, a clean output beam can be achieved only with the phase conjugation process. A situation exemplifying the second case occurs when the photorefractive crystal itself introduces phase aberrations in the pump and seed beams. In our experiment, we use two pieces of etched glass, one on each side of the photorefractive crystal, to simulate an extremely poor quality crystal and to demonstrate that the phase distortion caused by the aberrators is removed at the output port.

The experimental setup is shown schematically in Fig. 5. The output of an argon ion laser (4880Å) is spatially filtered, expanded to a diameter of 8 mm and weakly focused by lens L_1 at a distance of about 2.5 m. The beam is split by beamsplitter BS_1 into a strong pump beam and a weak seed beam with an intensity ratio of 95%:5%. The seed beam is directed by mirror M_1 to transmit through a SBN crystal onto the "a" face of a $BaTiO_3$ crystal, where the angle of incidence (ϕ) is 19° and the beam diameter is less than 1 mm. Polarization of the beams is such that extraordinary waves are excited in both crystals. This incident seed beam is phase-conjugated by the $BaTiO_3$ via the internal self-pump mode.[32] The phase-conjugate reflectance is approximately 14%. The pump beam transmitted through beamsplitter BS_1 and reflected by mirror M_2 is used to pump the phase-conjugated signal in the SBN crystal. The two beams enter the SBN crystal symmetrically, subtending an angle (θ) of 15° at the crystal. The diameter of each beam inside the crystal is about 2 mm. Two pieces of etched glass A_1 and A_2, one on each side of the SBN crystal, intercept the seed and pump beams, respectively, and introduce strong wavefront aberrations to the two beams. Mirror M_4, beamsplitters BS_3, BS_5 and BS_6 constitute a Mach-Zender interferometer for monitoring the wavefront of the incident beam after passing through the SBN crystal. The wavefronts of the pump beam and the amplified (phase-conjugated) signal are likewise monitored by the other two interferometers (M_5, M_6, BS_7, BS_8; and M_3, BS_2, BS_3, BS_4, respectively). The lenses used to project the fringes onto the screens (SC1, SC2 and SC3) are omitted in Fig. 5 for the sake of clarity. The SBN crystal is mounted on a linear translational stage so that it can be moved into (or out of) the beam paths.

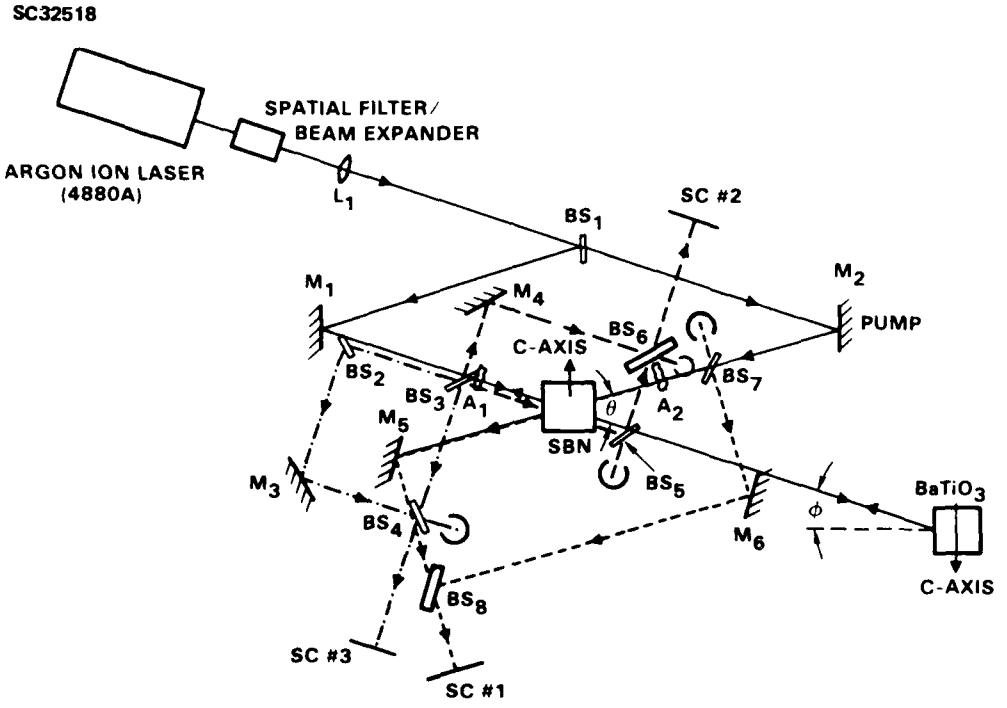

Fig. 5 Experimental setup for wavefront monitoring of two-wave mixing with phase conjugation.

With the SBN crystal and the two phase aberrators A_1 and A_2 removed, fringes representing wavefronts of the pump and seed beams, as monitored on screen SC1 and SC2, are shown in Fig. 6a and 6b, respectively. The circular fringe patterns in the figures indicate good quality (spherical) wavefronts. With the SBN crystal in place, fringes corresponding to wavefronts of the pump, the seed and the amplified (phase-conjugated) output are shown in Fig. 7a. Note that phase distortion introduced by the crystal is removed in the output. Figure 7b and 7c show the fringes when the phase aberrators A_1 and A_2 are introduced successively. Note that the output in Fig. 7c is relatively clean even when both the pump and seed beams are strongly aberrated. The residual distortion present in the amplified output is due mainly to scattering and absorption loss that is irreversible, and hence cannot be recovered. The intensity of the input beams and the phase-conjugated output corresponding to various cases shown in Fig. 7 is listed in Table 2-2. Note that the two-wave mixing gain drops from 20 to 10 for the case when both beams are strongly aberrated.

SC44565

(a) (b)

Fig. 6 Fringe pattern representing the primitive (nondistorted) wavefront of (a) the pump beam, and (b) the seed beam.

SC32511

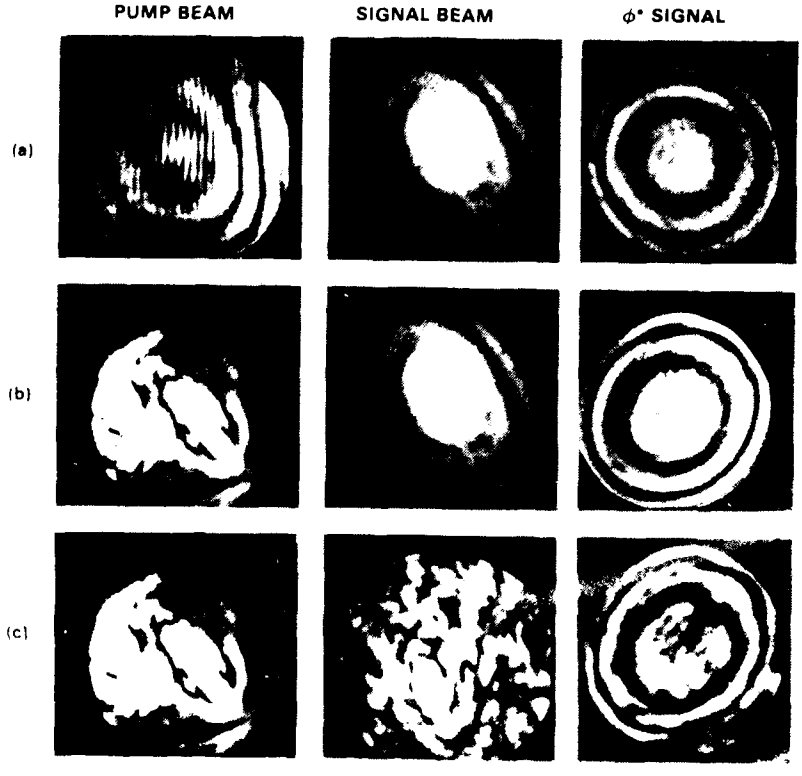

Fig. 7 Fringe patterns representing wavefronts of the pump, seed and the amplified (phase-conjugated) output (from left to right, respectively) for the case of (a) crystal imperfection, (b) strong pump aberration, and (c) strong aberration in both the pump and seed beams.

Table 2-2

Input and Output (Phase-Conjugate) Intensities and Gains

INPUT BEAM INTENSITIES

$I_P(0)$ = 90 mW (AVERAGE BEAM DIAMETER INSIDE SBN = 2 mm)
$I_S(0)$ = 2 mW (AVERAGE BEAM DIAMETER INSIDE SBN = 2 mm)

OUTPUT BEAM INTENSITIES AND GAIN

	WITHOUT PHASE DISTORTER	PUMP DISTORTED	BOTH PUMP & SIGNAL DISTORTED
$I_S(L)$	3.5 mW	3 mW	1.3 mW
$I_S'(L)$	0.17 mW	0.15 mW	0.13 mW
$g \equiv \frac{I_S(L)}{I_S'(L)}$	20	20	10

$I_S(L)$ = PHASE CONJUGATED SIGNAL OUTPUT WITH PUMP BEAM ON
$I_S'(L)$ = PHASE CONJUGATED SIGNAL OUTPUT WITH PUMP BEAM OFF
$g \equiv \frac{I_S(L)}{I_S'(L)}$ = SIGNAL GAIN

To summarize this section, we have demonstrated[33] the cleanup of a phase-aberrated laser beam by using photorefractive two-wave mixing in a SBN crystal in conjunction with self-pumped phase conjugation in a $BaTiO_3$ crystal. Using two-wave mixing, a clean seed beam is amplified by the phase-aberrated pump beam. The wavefront distortion introduced by the imperfection of the photorefractive crystal is eliminated via the phase conjugation process. This implies that although good optical quality photorefractive gain media are desirable for beam cleanup, poor optical quality media can be used provided the energy loss due to scattering and absorption is not severe enough to defeat the phase-conjugation process.

2.2.3 Relationships Between Electrostrictive Kerr Nonlinear Effects and Acousto-Optics

During our studies of the nonlinear Kerr processes, we began to analyze the electrostrictive nonlinearities. This mechanism of nonlinearity is of particular interest to us, since it is responsible for stimulated Brillouin scattering, and can be used for our experiments in nondegenerate two-wave mixing. We arrived at a number of interesting results, which to our knowledge have not been derived earlier. To summarize, we discovered some

relations which formally relate acousto-optic parameters of materials to their electrostrictive nonlinearities. We derived equations which prove that the electrostrictive coefficient, which is usually always treated in the literature as a scalar, is a fourth-rank tensor whose elements are closely related to the photoelastic parameters of the materials. Moreover, the electrostrictive contributions to the nonlinear index n_2 can be determined from the acousto-optic parameters and figures-of-merit. A surprisingly simple relation was obtained between the nonlinear index n_2 and M_3, an acousto-optic figure-of-merit defined to identify good candidate A-O materials for beam deflector applications.[34] This work, published in Ref. 7, Table 2-1, is believed to be very useful for estimating the electrostrictive contributions to the nonlinear index of materials. It also points out alternative means of determining the nonlinear properties of a medium, i.e., from its acousto-optic properties. It may become useful for us in the proposed continuation effort in materials selection.

Stimulated Brillouin Scattering (SBS)[35] has been widely used for optical phase conjugation[36] and other nonlinear effects.[35,37] Nonlinear SBS is based on the electrostrictive effect through which intense light interacts with the phonons in the medium. The relationships which exist between the electrostrictive Kerr effects and photoelastic phenomena are analyzed here. Also, we examined the fact that the electrostrictive coefficient γ, which is generally treated as a scalar, is a fourth rank tensor and is closely related to the material's photoelastic coefficients, and arrived at simplified relations which predict the value of the electrostrictive contribution to the nonlinear refractive index n_2 of the material, based on acousto-optical figures-of-merit. Conversely, using our derivations, information on the photoelastic properties of (electrostrictive) nonlinear materials may be obtained from the nonlinear properties.

The nonlinear index n_2 is defined by the relation

$$n = n_o + n_2 \langle E^2 \rangle = n_o + \frac{1}{2} n_2 E_m^2 \qquad (24)$$

where n_o is the linear refractive index, and $\langle E^2 \rangle$ is the time-averaged value of the square of the electric field. The parameter E_m is the electric field amplitude, as related to the optical intensity I by (in MKS system)

$$I = \frac{1}{2} \varepsilon_o n_o c E_m^2 \quad , \qquad (25)$$

where ε_o and c are the vacuum permittivity and velocity of light, respectively. The strength of stimulated Brillouin scattering, as well as nonlinear self-focusing, depend strongly on the value of n_2. An important contribution to n_2 is due to the electrostrictive properties of the medium, as generally stated[38] by

$$P = -\frac{1}{2}\gamma \langle E^2 \rangle \quad , \tag{26}$$

where P is the electrostrictive pressure. Beginning with the above equations, we derive the expressions relating the electrostrictive Kerr effects to the acousto-optic properties of the medium. Some interesting relationships are obtained which can be useful for material selection in nonlinear optics and for characterization of materials.

Electrostrictive and Photoelastic Effects

The simple relation given in Eq. (26) relates the effects of electric fields to the electrostrictive pressure P. The electrostrictive pressure causes strain in the medium, as the stress and strain components are related by the stiffness constants $C_{ijk\ell}$. Here, we derive a simple relationship which demonstrates the connection between the electrostrictive and photoelastic properties of a liquid. A more generalized treatment for anisotropic media is given in Appendix B.

The photoelastic effect occurs in all states of matter; it is analytically described[39] by a fourth rank tensor $p_{ijk\ell}$ which couples the strain tensor $S_{k\ell}$ to changes in the indicatrix $(1/n^2)_{ij}$

$$\Delta\left(\frac{1}{n^2}\right)_{ij} = p_{ijk\ell}\, S_{k\ell} \quad , \tag{27}$$

where the summation over the repeated indices k and ℓ is implicit. Using the derivative, we obtain

$$\Delta n = -\frac{1}{2} n^3\, p\, S \quad . \tag{28}$$

Here, for simplicity, we have considered the case of a uniaxial strain in a liquid. Similarly, we can relate the electrostrictive coefficient to the changes in the index by the relation[4] defining γ as

$$\gamma \equiv \rho \frac{\partial \varepsilon}{\partial \rho} = 2\varepsilon_o \rho n \frac{\partial n}{\partial \rho} \quad , \tag{29}$$

where ρ is the material density, and $\varepsilon = \varepsilon_o n^2$ is the high frequency dielectric constant of the medium. Taking the derivative, we obtain

$$\Delta n = \left(\frac{\gamma}{2n\varepsilon_o}\right)\left(\frac{\partial \rho}{\rho}\right) = -\frac{\gamma}{2n\varepsilon_o} S \quad , \tag{30}$$

where again we have assumed uniaxial strain in a liquid. Equating the change in index from Eqs. (28) and (30) we obtain, for the case of uniaxial strain in a liquid, a scalar relationship

$$\gamma = \varepsilon_o n_o^4 p \quad . \tag{31}$$

A more rigorous treatment for the most general case, including anisotropic media, similarly relates the components of the two fourth rank tensors γ and p (see Appendix B):

$$\gamma_{ijk\ell} = \varepsilon_o n^2_k n^2_\ell p_{k\ell ij} \tag{32}$$

Two ramifications of Eq. (32) are interesting: first, acousto-optic materials may be found to be useful as nonlinear materials in applications such as stimulated Brillouin scattering, in which electrostriction is important. Later in this paper, we will examine this connection of acousto-optics and nonlinear electrostrictive effects. Second, one can obtain data on components of γ (from the acousto-optic data) or $P_{ijk\ell}$ (from electrostrictive data) that have not been obtained to date. Since the electrostrictive coefficient has been generally treated as a scalar, there is a lack of information about the numerous components of γ in solids. Table 2-3 shows an example of data inferred from Eq. (32) using data found in the literature;[40] often, data can only be found on the photoelastic tensor elements $p_{ijk\ell}$. The indices, i,j,k,ℓ = 1, ...3 can also be reduced to two indices using the reduced index[40] notation, where i,j = 1, ... 6.

Table 2-3

Calculated Values for Electrostrictive Tensor Elements Using Photoelastic Data (from Ref. 40) for Selected Materials and Eq. (32)

Material	n	p_{ij}‡	γ_{ij}‡	γ_{ij} (MKS)‡
Fused Silica	1.46	$p_{11} = 0.121$ $p_{12} = 0.27$	$\gamma_{11} = 0.55\ \varepsilon_o$ $\gamma_{22} = 1.23\ \varepsilon_o$	$\gamma_{11} = 4.87 \times 10^{-12}$ $\gamma_{21} = 1.09 \times 10^{-11}$
Water	1.33	$p_{11} = p_{12} = 0.31$	$\gamma_{11} = \gamma_{21} = 0.97\ \varepsilon_o$	$\gamma_{11} = \gamma_{21} = 8.6 \times 10^{-12}$
$PbMoO_4$ (long)	$n_o = 2.39$ $n_e = 2.26$	$p_{11} = p_{12} = 0.24$ $p_{33} = 0.29$	$\gamma_{11} = \gamma_{21} = 7.0\ \varepsilon_o$ $\gamma_{33} = 8.5\ \varepsilon_o$	$\gamma_{11} = \gamma_{21} = 6.2 \times 10^{-11}$ $\gamma_{33} = 7.5 \times 10^{-11}$
Ge	4.0	$p_{11} = 0.27$	$\gamma_{11} = 69.1\ \varepsilon_o$	$\gamma_{11} = 6.1 \times 10^{-10}$
CS_2*	1.63	$p_{12} \sim 0.66$	$\gamma_{21} \sim 4.6\ \varepsilon_o$	$\gamma_{21} \sim 4 \times 10^{-11}$

‡ Values shown for the electrostrictive tensor elements are given both in units of ε_o and MKS units. The reduced index notation is also used.
* Value for CS_2 estimated from experimental A-O data.

Nonlinear Index and Acousto-Optical Parameters

We begin by examining Eq. (24) in terms of the nonlinear index n_2:

$$n_2 = \frac{\partial n}{\partial \langle E^2 \rangle} \quad . \tag{33}$$

Differentials of both sides of Eq. (26) will yield

$$dP = -\frac{1}{2}\,\gamma\, d\langle E^2 \rangle \quad . \tag{34}$$

We now use the definition of bulk modulus B

$$B = -\rho \frac{\partial P}{\partial \rho} \quad , \tag{35}$$

and substitute the value of $\rho/d\rho$ in Eq. (35) from Eq. (29). Solving for dP, we obtain

$$dP = \frac{-2\varepsilon_o nB}{\gamma} \cdot dn \quad . \tag{36}$$

Equating the right-hand side of Eqs. (24) and (36), and solving for n_2 using Eq. (26), we arrive at the expression for n_2 in terms of the electrostrictive coefficient γ

$$n_2 = \frac{\gamma^2}{4\varepsilon_o Bn} \quad , \tag{37}$$

which in turn, from Eq. (31), can be rewritten in terms of the photoelastic constants p

$$n_2 = \frac{n^7 \varepsilon_o p^2}{4B} \quad . \tag{38}$$

Equation (38) is interesting in that one can readily calculate values for the electrostrictive contribution to the nonlinear index from photoelastic data,[34] and compare these figures with values of n_2 obtained from data on the phase shift of light as a function of intensity.[41] Deviations can be interpreted in terms of the relative electrostrictive contribution to the total nonlinear index. Although data on $P_{ijk\ell}$ are available, it is easier to determine n_2 from acousto-optic figures-of-merit, as shown below.

Acousto-optic (A-O) properties of materials are in many cases reported in terms of certain figures-of-merit, commonly referred to as M_1, M_2 or M_3, each defined for a specific A-O application. For example, A-O efficiency η of an optical beam which is Bragg-reflected from an acoustic beam can be shown by[39]

$$\eta = \sin^2 \left[\frac{\pi L}{\lambda \cos\theta} \left(\frac{P_{ac}}{2HW} \cdot \frac{n^6 p^2}{\rho V^3}\right)^{1/2}\right] \tag{39}$$

where P_{ac} is the acoustic power, H and W are the dimensions of the acoustic transducer, L is the interaction length, θ is the Bragg angle, λ is the wavelength, ρ is the density, p is the relevant photoelastic constant, and V is the velocity of the acoustic wave. A general practice has been to lump all of the parameters on the right-hand side of Eq. (39) which depend on the material properties into a figure-of-merit M_2:

$$M_2 = \frac{n^6 p^2}{\rho V^3} \quad . \tag{40}$$

This is the most widely used A-O figure-of-merit and is used for material selection and comparisons for general A-O applications. Two other figures-of-merit, M_1 and M_3, are used for specialized applications. Of particular interest to us is M_3,

$$M_3 = \frac{n^7 p^2}{\rho V^2} \quad . \tag{41}$$

This figure-of-merit is used for comparison of A-O materials for applications where specific bandwidths and optical apertures are desired (e.g., A-O beam deflectors). As we will show below, both M_2 and M_3 can also yield values for electrostrictive nonlinear coefficients. Using Eqs. (38), (40), (41) and the fact that the bulk modulus B is related to the sound velocity in the medium ($B = \rho V^2$),[38] we can demonstrate that the nonlinear index n_2 can be related to the A-O figures-of-merit:

$$n_2 = \frac{1}{4} n_o \varepsilon_o V M_2 \quad , \quad \text{or} \tag{42}$$

$$n_2 = \frac{1}{4} \varepsilon_o M_3 \quad . \tag{43}$$

The above equations are very useful in order to evaluate quickly the A-O materials for their electrostrictive nonlinear properties. Table 2-4 shows the relative merit of a number of A-O materials in terms of nonlinear coefficient n_2 given in both MKS and esu systems of units. M_3 values from Ref. 6 have been used to determine n_2 using Eq. (43).

The relationships given in Eqs. (38), (42) and (43) are very useful since considerable data on A-O properties of materials are accessible. In contrast, specific data for electrostrictive nonlinearities are largely not available. The n_2 values reported in the literature[41] in many cases are inclusive of several mechanisms, including molecular orientation, molecular redistribution, nonlinear electronic polarizability, thermal and electrostrictive.

Table 2-5 shows electrostrictive n_2 values calculated from Eq. (43) for selected materials in comparison with those obtained by interferometric measurements of phase shift as a function of intensity from Ref. 41. Comparisons indicate that the nonlinearities in CS_2 are probably entirely electrostrictive, whereas for fused silica, NaCl, and Ge, this

Table 2-4

Values of Electrostrictive Nonlinear Index n_2 Derived from Acousto-Optic Figure-of-Merit M_3 for Selected Materials

Material	M_3*	n_2 (MKS)	n_2 (esu)
Fused Silica	1.3×10^{-12} (cgs) 1.3×10^{-11} (MKS)	2.9×10^{-23}	2.6×10^{-14}
Water	2.91×10^{-11} (cgs) 2.91×10^{-10} (MKS)	6.4×10^{-22}	5.8×10^{-13}
TeO_2 (long.)	3.47×10^{-11} (cgs)	7.7×10^{-22}	6.9×10^{-13}
Ge	1.7×10^{-9} (cgs) 1.79×10^{-8} (MKS)	4.0×10^{-20}	3.6×10^{-11}
CS_2	6.2×10^{-9} (MKS)	1.4×10^{-20}	1.2×10^{-11}

n_2 (esu) = 9×10^8 n_2 (MKS)
* From Ref. 34

Table 2-5

Comparison of Calculated Electrostrictive Contribution to the Nonlinear Index n_2 with Experimental Data on Total n_2 for Selected Materials (from Ref. 41)

Material	Experimental n_2 (esu)	Calculation* n_2 (esu)
Fused Silica	1×10^{-13}	2.6×10^{-14}
NaCl	1.2×10^{-13}	3.8×10^{-14}
Ge	1.4×10^{-9}	3.6×10^{-11}
CS_2	1.1×10^{-11}	1.2×10^{-11}
Water	9×10^{-14}	5.8×10^{-13}

* From Acousto-Optic parameters (Ref. 34) and Eq. (43).

contribution is only a part of the overall n_2. Assuming that the differences in n_2 values for water are accurate, then the nonelectrostrictive nonlinearities in water are apparently opposite in sign to the electrostrictive term. We have applied our theory to limited examples. There is considerable data in the literature which can be used to probe the nature and strength of electrostrictive nonlinearities in various media.

It should be pointed out that the calculated electrostrictive n_2 values from our relationships are nonresonant values. In nonlinear optical mixing of high power beams, it is possible to achieve resonance with the acoustic phonons in the medium. Depending on the acoustic attenuation of the particular sound waves, significant increase in the effective n_2 is possible. For example, in conventional SBS, resonance enhancements of n_2 are observed when the phase conjugation process is in resonance with the sound waves.

In summary, we have analyzed the relationships that exist between electrostrictive and photoelastic properties of media, and related these parameters to the electrostrictive contribution to the nonlinear index n_2. We have also derived new relations which can be used to readily obtain n_2 values for a large number of acousto-optic materials for which A-O figures-of-merit are available.

2.2.4 Nondegenerate Two-Wave Mixing Experiments

We carried out numerous experiments to demonstrate artificial photorefractive effects by nondegenerate two-wave mixing (NDTWM) in Kerr media. The majority of these experiments used CS_2 as the nonlinear medium. Figure 8 shows a schematic diagram of the NDTWM experiments. We achieved stimulated Brillouin scattering when we desired but found that the conditions of the NDTWM were more stringent than originally thought, particularly if the resonance effects that were considered in the theory were to be achieved.

The conditions for resonance are met when the wave-vector and frequency difference of the two optical beams give rise to interference fringes that travel exactly at the velocity of the acoustic phonons needed to match the energy exchange process (see Sect. 2.2.1). When this condition of resonance is met, a spatial phase difference of $\pi/2$ automatically appears between the intensity pattern and its nonlinear holograms, maximizing the energy exchange process. As it turns out, the acoustic vibrations in the medium are

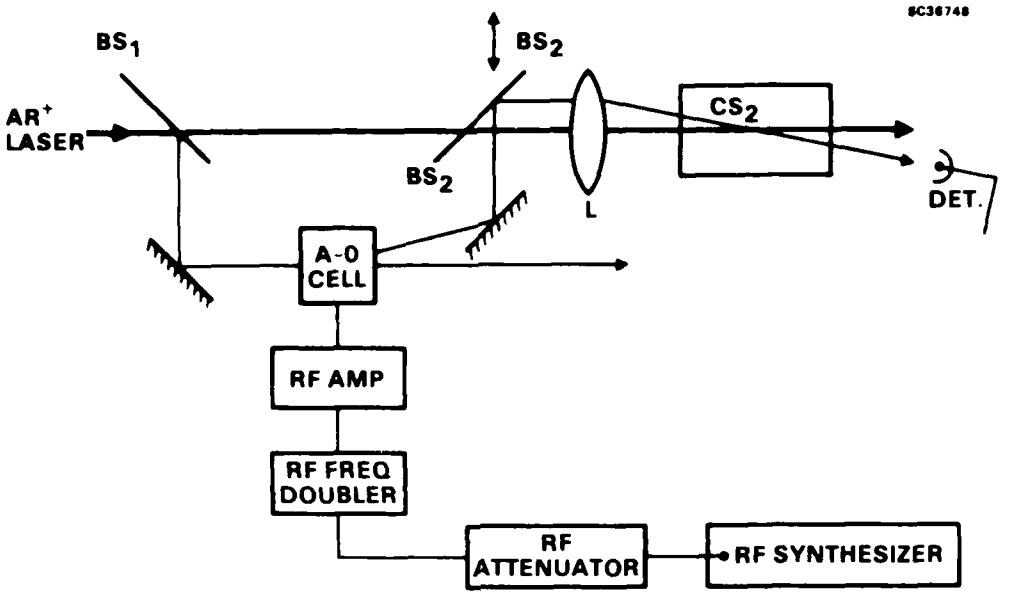

Fig. 8 Schematic diagram of the nondegenerate two-wave mixing experiments. The input beam is mixed in a nonlinear medium with a frequency shifted portion which has been diffracted and frequency shifted, using an acousto-optic cell.

fairly high quality resonators, particularly at the frequencies that we were using ($\Delta f \leq 250$ MHz). This makes the conditions of the experiments in terms of the mixing angle, beam shapes and beam overlap, and stability, rather critical. Moreover, the nonlinear optically generated acoustic waves can result in considerable additional gains if the optical aperture is large enough to allow a buildup. Our experiments, however, are energy limited to about 1 J per pulse. Therefore, the beams need to be focused to achieve threshold intensities, sacrificing the resonance buildup. The primary difficulty here was found to be insufficient pulse energies.

Our NDTWM experiments were stopped in favor of the new concept of Kerr-Bragg effect which was developed as a means of reducing the problem of critical alignments, and reducing the energy thresholds. It is becoming increasingly clear that the concepts that we are pursuing require large photon fluxes in order to achieve the nonlinear response desired. This is in line with our general goal of applying our concepts to SDI needs. In the future (proposal) Phase II of the program, described in Section 3, we plan to carry out experiments on both Kerr-Bragg and NDTWM effects using higher energy lasers.

2.2.5 Kerr-Bragg Effect

The Kerr-Bragg (K-B) concept was developed as a variation of the general NDTWM experiments shown in Fig. 8. The basic concept (described in Ref. 4, Table 2-1) involves carrying out the frequency shifting and seed beam generation inside of the nonlinear medium itself, rather than outside. This would ensure automatic matching of the proper angle and frequency shift, and based on acoustic considerations, a lower optical energy threshold would be expected. Figure 9 shows a schematic drawing of the general K-B concept.

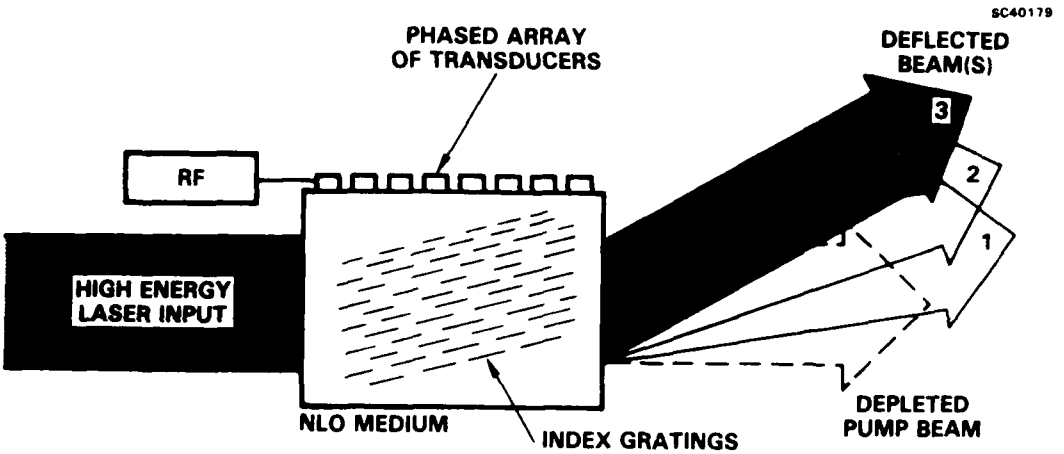

Fig. 9 Schematic diagram of the Kerr-Bragg concept. Initial beam diffraction is by the acoustic waves, which are subsequently amplified by two-wave mixing.

The K-B process is very attractive for SDI applications because it allows the well-established acousto-optic device concepts to be extended to high energy applications. The concept actually only works at high laser energies.

2.2.5.1 Kerr-Bragg Modeling

We carried out detailed analytic modeling of the K-B process. This work was published in Ref. 8, Table 2-1. The nonlinear response of acousto-optic Bragg scattering due to Kerr effect was considered. The problem was formulated by a coupled-mode theory. An exact expression for the diffraction efficiency as a function of the optical intensity was obtained. We showed that the diffraction efficiency is a nonlinear function of the intensity of the incident optical beam. This work will be of considerable help to us in the proposed effort to carry out more detailed modeling of the nonlinear processes for beam steering.

Acousto-optic Bragg scattering is a well-known phenomenon and has been widely used for beam steering, beam modulation, frequency shifting, and other applications. It is a physical process in which an incident laser beam is scattered from an acoustic field. The scattered beam is shifted in frequency by an amount which is exactly the frequency of the acoustic field. In addition, the scattered beam propagates along a new direction which is determined by the Bragg condition.[42]

If the Bragg cell is made of a nonlinear optical medium, the incident beam and the scattered beam form a travelling interference pattern which may induce a volume index grating. Such a volume index grating will then affect the propagation of these two beams. If the optical nonlinearity of the medium is due to the electrostrictive Kerr effect, then an additional sound wave can be generated due to the two-beam coupling. This additional sound wave is added to the applied acoustic field and thus enhances the diffraction efficiency.

From the quantum mechanical point of view, for each photon scattered, there is one phonon generated or annihilated depending on whether the frequency is down-shifted or up-shifted. In the case of frequency down-shift, there is one phonon generated for each photon scattered. Thus the number of generated phonons is proportional to the scattered intensity. For low intensity light, these additional phonons are much smaller in number relative to the phonons of the applied acoustic field. However, for high intensity laser beams, the number of generated phonons can be much larger than those of the applied acoustic field. The presence of these additional phonons effectively enhances the acoustic field and thus increases the diffraction efficiency.

Both acousto-optic Bragg scattering and nondegenerate two-wave mixing in Kerr media have been individually treated by previous scientists.[42,43] In addition, the amplification of sound waves through the interaction of two laser beams with different frequencies has been observed experimentally.[44] To the best of our knowledge, the coupling between the Bragg scattered beam and the incident beam due to Kerr effect has never been studied. Such coupling leads to nonlinear optical Bragg scattering. In a Bragg cell with a low acoustic field, the diffraction efficiency may be low at low optical intensity. When the optical intensity is above some threshold, the phonon regenerative process leads to an avalanche in which all the photons are diffracted. This report presents a coupled mode theory of the nonlinear optical Bragg scattering in Kerr media. An exact solution is obtained for the nonlinear diffraction efficiency.

Theoretical Formulation

Consider the propagation of two optical plane waves in a Kerr medium. Following the notation used in Ref. 43, the electric field of the two waves is written

$$E_j = A_j \exp[i(\omega_j t - \vec{k}_j \cdot \vec{r})] \qquad j = 1,2 \qquad (44)$$

where ω_j's are the frequencies and $\vec{k}_j$'s are the wave vectors. In Eq. (1), we assume for simplicity that both waves are s-polarized and the medium is isotropic. We further assume that no optical rotation is present in the material. A_1 and A_2 are the amplitudes and are taken as functions of z only for a steady-state situation. The z-axis is taken normal to the surface of the medium (see Fig. 10).

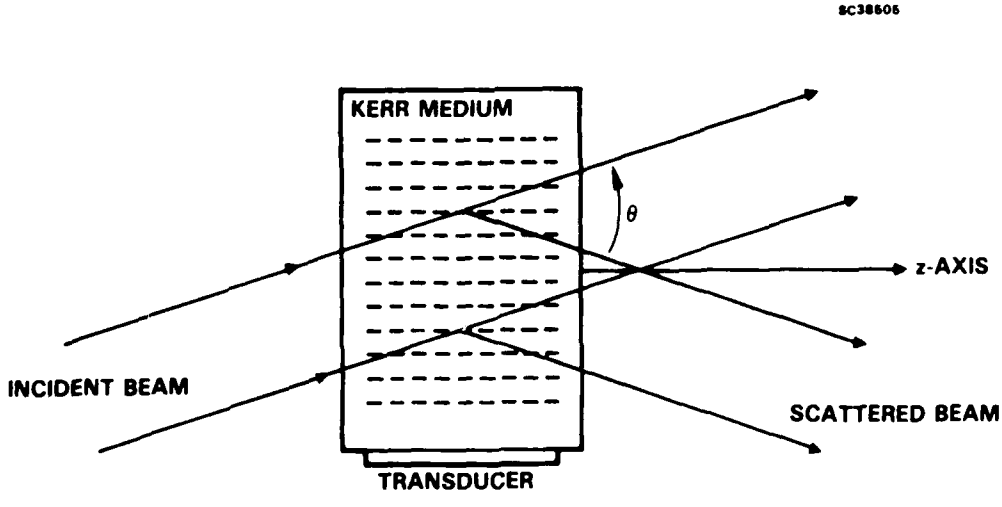

Fig. 10 Schematic diagram of nonlinear Bragg scattering in Kerr media.

In the Kerr medium, these two waves generate an interference pattern which induces a volume index grating. The fundamental component of the induced grating can be written

$$\Delta n = \frac{1}{2}\{n_2 e^{i\phi} A_1 A^*_2 e^{i(\Omega t - \vec{K}\cdot\vec{r})} + \text{c.c.}\} \tag{45}$$

where ϕ and n_2 are real, and $\Omega = \omega_1 - \omega_2$, $\vec{K} = \vec{k}_1 - \vec{k}_2$. Here, again, for the sake of simplicity, we assume a scalar grating. The phase ϕ indicates the degree to which the index grating is temporally delayed (or spatially shifted) with respect to the interference pattern. We may regard $n_2 \exp(i\phi)$ as a complex Kerr coefficient. Generally speaking, both n_2 and ϕ are functions of Ω and $\vec{K}$. For media whose Kerr effect is dominated by electrostriction, such a complex Kerr coefficient can be written[35]

$$n_2 e^{i\phi} = \frac{-K^2\gamma^2}{4n\rho\varepsilon_0(\Omega^2 - v^2K^2 - i\Omega\Gamma)} \tag{46}$$

where γ is the electrostrictive coefficient, v is the acoustic velocity, ρ is the mass density, n is the index of refraction of the medium, ε_0 is the dielectric constant of the vacuum, and Γ is the inverse of the phonon lifetime. We notice that the Kerr coefficient is purely imaginary when $\Omega = \pm vK$. The n_2 in Eq. (46) should not be confused with the nonresonant value ($\Omega = 0$) which is responsible for self-focusing and intensity-induced phase shifts.[41]

If an acoustic field is applied such that the wave A_2 is generated by scattering of the wave A_1 from the sound wave, then the condition $\Omega = \pm vK$ is automatically satisfied provided that the wave A_1 is incident along a direction which satisfies the Bragg condition. Under these circumstances, the coupled mode equations that govern the propagation of these two waves in the medium can be written

$$\frac{d}{dz}A_1 = -\frac{1}{2}g|A_2|^2A_1 - i\kappa A_2$$

$$\frac{d}{dz}A_2 = \frac{1}{2}g|A_1|^2A_2 - i\kappa^* A_1 \tag{47}$$

where κ is the Bragg coupling constant,[42] and g is the Kerr intensity coupling constant which is given by[43]

$$g = \frac{2\pi n_2}{\lambda \cos(\theta/2)} \sin\phi \tag{48}$$

where λ is the wavelength, and θ is the angle between the beams in the medium. This angle θ is twice the Bragg angle θ_B ($2k \sin\theta_B = K$). The phase ϕ is either +90 or -90° depending on the sign of $\Omega = \omega_2 - \omega_1$. For the case when beam 2 is scattered with a frequency down-shift, the phase ϕ is +90° indicating a gain for beam 2.

We now write

$$A_1 = \sqrt{I_1} e^{i\psi_1} \quad , \quad A_2 = \sqrt{I_2} e^{i\psi_2} \tag{49}$$

where ψ_1 and ψ_2 are the phases of the amplitudes A_1 and A_2, respectively. Using Eq. (48), the coupled equations can be written

$$I_1' + 2I_1 i\psi_1' = -gI_1I_2 - 2i\kappa\sqrt{I_1I_2}\; e^{i(\psi_2-\psi_1)}$$

$$I_2' + 2I_2 i\psi_2' = gI_1I_2 - 2i\kappa^*\sqrt{I_1I_2}\; e^{i(\psi_1-\psi_2)} \quad , \tag{50}$$

respectively, where the prime indicates a differentiation with respect to z.

By rewriting κ as $\kappa \exp(i\sigma)$ so that κ is now a positive number and splitting the real and imaginary parts, we obtain

$$I_1' = -gI_1I_2 + 2\kappa\sqrt{I_1I_2} \sin\Delta\psi$$

$$I_2' = gI_1I_2 - 2\kappa\sqrt{I_1I_2} \sin\Delta\psi \tag{51}$$

and

$$\psi_1' = -\kappa(I_2/I_1)^{1/2} \cos\Delta\psi$$

$$\psi_2' = -\kappa(I_1/I_2)^{1/2} \cos\Delta\psi \tag{52}$$

where

$$\Delta\psi = \psi_2 - \psi_1 + \sigma \tag{53}$$

These equations are very similar to those describing mode coupling in ring laser gyros.[45,56] In fact, the relative phase between the waves can be written, according to Eqs. (52) and (53)

$$\Delta\psi' = -\kappa[(I_1/I_2)^{1/2} - (I_2/I_1)^{1/2}]\cos\Delta\psi \tag{54}$$

which is similar to the well-known phase coupling equations in ring laser gyros. In our case, since the wave A_2 is generated by Bragg scattering of the wave A_1 from the acoustic field, it is legitimate to assume that the phase of A_2 is connected to that of the incident wave A_1. Thus

$$\Delta\psi = \pi/2 \quad , \quad 3\pi/2 \tag{55}$$

are good solutions of Eq. (54).

For $g = 0$, exact solution of the coupled Eq. (47), subject to the boundary condition of $A_2(0) = 0$, yields a relative shift of $\Delta\psi = 3\pi/2$. We will take this as the proper solution to Eq. (54). Substitution of $\Delta\psi = 3\pi/2$ into Eq. (51) leads to

$$\begin{aligned} I_1' &= -gI_1I_2 - 2\kappa\sqrt{I_1I_2} \\ I_2' &= gI_1I_2 + 2\kappa\sqrt{I_1I_2} \end{aligned} \tag{56}$$

The coupled Eqs. (56) can be integrated exactly, and the solution is

$$I_1(z) = I\cos^2 u \tag{57}$$

$$I_2(z) = I\sin^2 u$$

where I is the incident intensity at $z = 0$ (i.e., $I_1(z) = I$ and $I_2(z) = 0$ at $z = 0$), and u is given by (see Appendix C)

$$\tan u = \frac{\tan (\kappa z\sqrt{1 - b^2})}{\sqrt{1 - b^2} - b \tan(\kappa z\sqrt{1 - b^2})} \tag{58}$$

with

$$b = \frac{gI}{4\kappa} = \frac{\gamma L}{4\kappa L} \tag{59}$$

where $\gamma = gI$ and L is the length of interaction. We note that b is a dimensionless parameter which is the ratio of Kerr coupling to Bragg coupling. Equation (58) is valid for all values of b. When the magnitude of b becomes greater than 1 (i.e., $|b| > 1$), $\sqrt{1 - b^2}$ becomes $i\sqrt{b^2 - 1}$ and $\tan \kappa z\sqrt{1- b^2}$ becomes $i \tanh \kappa z\sqrt{b^2 - 1}$. We also note that κ is a positive number as defined earlier. The Kerr coupling constant g can be either positive or negative depending on whether the frequency of beam 2 is down-shifted or up-shifted.

We now examine the intensity variation with respect to z for various values of b. For $b > 1$, $I_2(z)$ reaches its maximum value I (100% energy transfer) at distance z such that $\tanh (\kappa z\sqrt{b^2 - 1}) = \sqrt{b^2 - 1}/b$. Beyond this point, the intensity $I_2(z)$ decreases and reaches its asymptotic value of $I/[2b(b - \sqrt{b^2 - 1})]$ which becomes I when b approaches infinity.

For $b = 1$, $I_2(z)$ reaches its maximum value I at $z = 1/\kappa$. Beyond this point, the intensity $I_2(z)$ decreases and reaches its asymptotic value of I/2 at $z = \infty$.

For $0 \le b < 1$, $I_2(z)$ is a periodic function of z with maximum value I at points when $\tan (\kappa z\sqrt{1 - b^2}) = \sqrt{1 - b^2}/b$. The minimum value of $I_2(z)$ is zero which occurs when $\tan (\kappa z\sqrt{1 - b^2}) = 0$. Notice that maximum or minimum occurs when $I_1 I_2 = 0$.

For $-1 < b < 0$ $I_2(z)$ is also periodic function of z with maximum value I at points when $\tan (\kappa z\sqrt{1 - b^2}) = \sqrt{1 - b^2}/b$. Compared with the case $0 \le b < 1$, we notice that it takes a longer interaction length for I_2 to reach its maximum value because of the negative Kerr coupling. Minimum value of $I_2(z)$ is zero which also occurs when $\tan (\kappa z\sqrt{1 - b^2}) = 0$.

For $b = -1$, $I_2(z)$ is a monotonically increasing function of z with an asymptotic value of $I_2(z) = I/2$ at $z = \infty$. For $b < -1$, $I_2(z)$ is also a monotonically increasing function of z with an asymptotic value of $I_2(z) = I/(2b^2 - 2b\sqrt{b^2 - 1})$ at $z = \infty$. Figure 11 plots the intensity of $I_2(z)$ as a function z at various values of b.

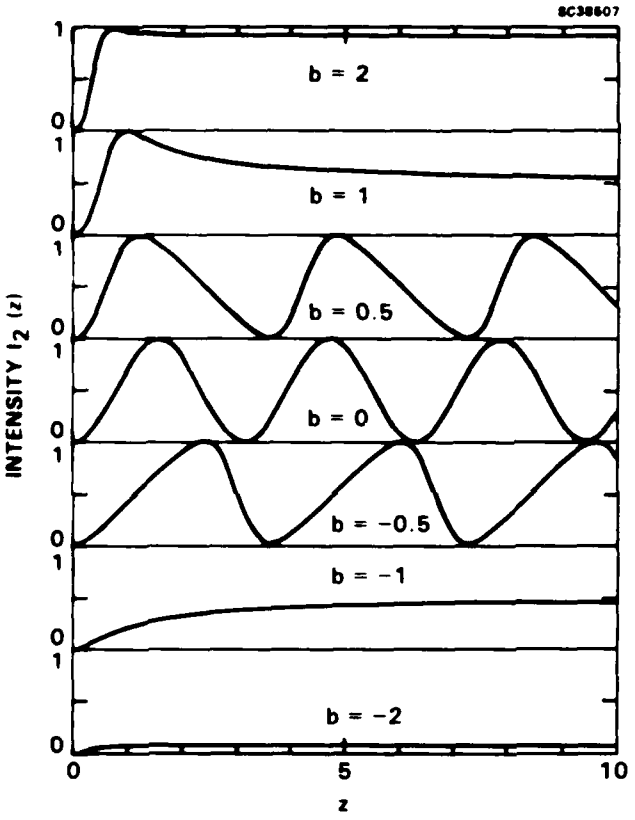

Fig. 11

Intensity variation of the scattered beam $I_2(z)$ as a function of z for various values of b.

We now examine the diffraction efficiency which is defined as

$$\eta = \frac{I_2(L)}{I} = \sin^2 u \tag{60}$$

as a function of intensity I (or b) for a given Bragg coupling constant κ and a length of interaction L. Figure 12 plots the diffraction efficiency η as a function of the parameter b for various values of κL. We notice that for $b > 0$ (or $g > 0$) the diffraction efficiency η is an increasing function of intensity and can reach nearly 100% at high optical intensities. The enhancement in the diffraction efficiency due to strong Kerr coupling can be employed for the steering of high power lasers.

When $b \gg 1$ and $b\kappa L \gg 1$, the asymptotic expression for the diffraction efficiency is, according to Eqs. (58) and (60)

$$\eta = 1 - 4b^2 \exp(-4\kappa L b) \tag{61}$$

we notice that the diffraction efficiency approaches 100% exponentially at large b (high intensity). When b approaches $-\infty$, the asymptotic form of the diffraction efficiency is, according to Eqs. (58) and (60)

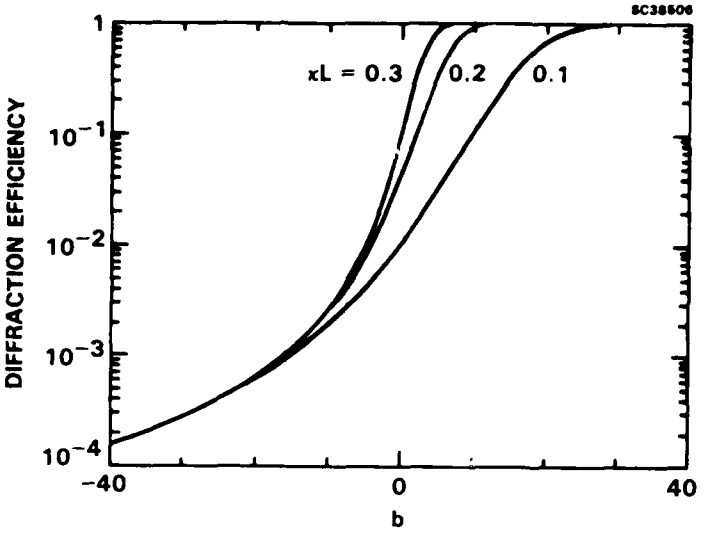

Fig. 12 Diffraction efficiency η as a function of the parameter b for various values of κL.

$$\eta = \frac{1}{4b^2}\left[1 - 2\exp\left(-2\kappa L|b|\right)\right] \tag{62}$$

According to Eqs. (59) and (61), for small κL, high diffraction efficiency occurs when $\gamma L >> 1$ (or $gIL >> 1$) which corresponds to the Kerr regime. However, the diffraction efficiency is zero when $\kappa L = 0$, according to Eqs. (58) and (60).

At $b = 0$, Eq. (60) reduces to $\eta = \sin^2 \kappa L$ which is the familiar expression of the Bragg cell diffraction efficiency.

To observe such nonlinear Bragg scattering, the Kerr coupling constant must be comparable with the Bragg coupling constant. Thus, the parameter b must be of the order of 1. Using $b = 1$ as an example, the Kerr intensity coupling constant must be

$$gI = 4\kappa. \tag{63}$$

We now take a Bragg coupling constant of $\kappa = 1\ cm^{-1}$ as an example and use a nonlinear medium such as CS_2. Using the data available in Ref. 35, the Kerr coupling constant g for a Bragg angle of 5° ($2\theta = 10°$) is $g = 1.5$ cm/MW and the rf frequency required is 640 MHz. Thus, the optical intensity needed to observe a significant nonlinearity in Bragg scattering, according to the condition in Eq. (63), is approximately 2.7 MW/cm^2.

To summarize this section, we have considered the nonlinear response of acousto-optic Bragg scattering due to Kerr effect. The problem was formulated by using a coupled mode theory, and exact solutions for the intensity variation were obtained. The results show that diffraction efficiency is a nonlinear function of the optical intensity and can be greatly enhanced by increasing the intensity of optical wave. It can be used as a nonlinear device in which high efficiency diffraction only occurs when the optical intensity is above a threshold.

2.2.5.2 Kerr-Bragg Demonstration

The Kerr-Bragg process in principle is very simple. However, it took many unsuccessful experiments (in the visible and infrared) to teach us the actual complexities involved in the experiment before we could succeed. For example, the current theoretical modeling can not be directly used to predict the results of the experiments, because of the approximations used. Moreover, there are thermal and competing nonlinear effects that interfere with the experiments. The most severe problem, however, turned out to be the fact that the laser energies available to us (~ 1 J per pulse) are not sufficient for dramatic energy exchange effects. Deviations of the laser beam profile from a gaussian shape to higher order spatial modes cause problems, and corrections can not be made without further loss of laser beam energy.

After we came to a better understanding of the experimental requirements, a successful demonstration was made that shows the predicted nonlinear acousto-optic (K-B) effect. Figure 13 shows a schematic diagram of the experimental setup. The effect was seen in fused quartz, which is the material of the A-O cell used for the experiment. The acoustic frequency was near 85 MHz, and the laser was a pulsed Nd:YAG laser which could be Q-switched to produce pulses of about 8-30 ns, at 10 to 20 Hz repetition rate. The pulse widths for non-Q-switched operation are near 100 μs, and the pulse energies are adjustable up to a maximum of nearly 1 J, for any mode of operation.

Figures 14 show the results of measurements of the A-O diffraction efficiency plotted versus laser pulse energy. Both the Q-switched and non-Q-switched cases show an increase of the diffraction efficiency with the increasing pulse energy. No such increase is expected if nonlinear optical effects are not stimulated. The nonlinear response for the non-Q-switched case is somewhat higher. This effect is under further study, but the general

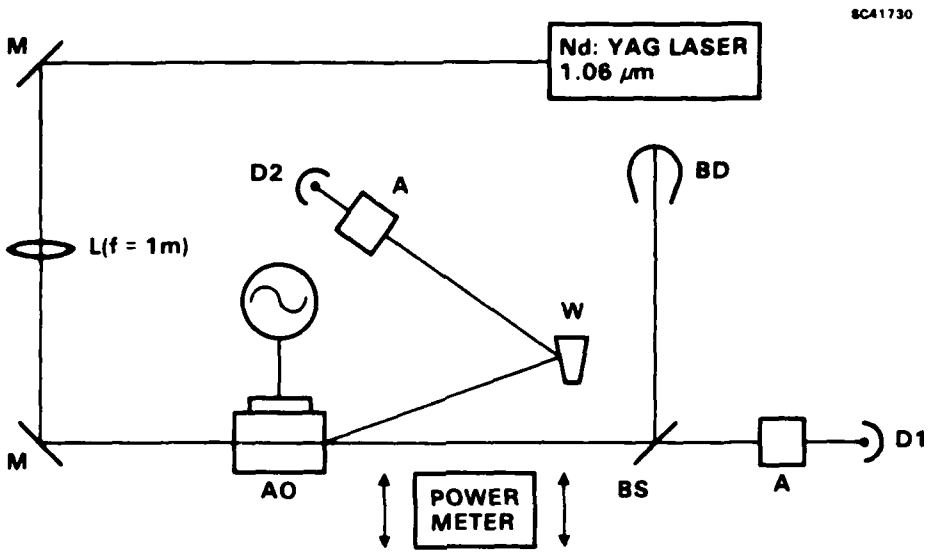

Fig. 13 Schematic drawing of the Kerr-Bragg demonstration setup. BD = Beam Dump; W = Wedge beam splitter; A = Attenuator; BS = Beam Splitter; AO = Acousto-Optic cell; M = Mirror, D1, D2 = Detectors.

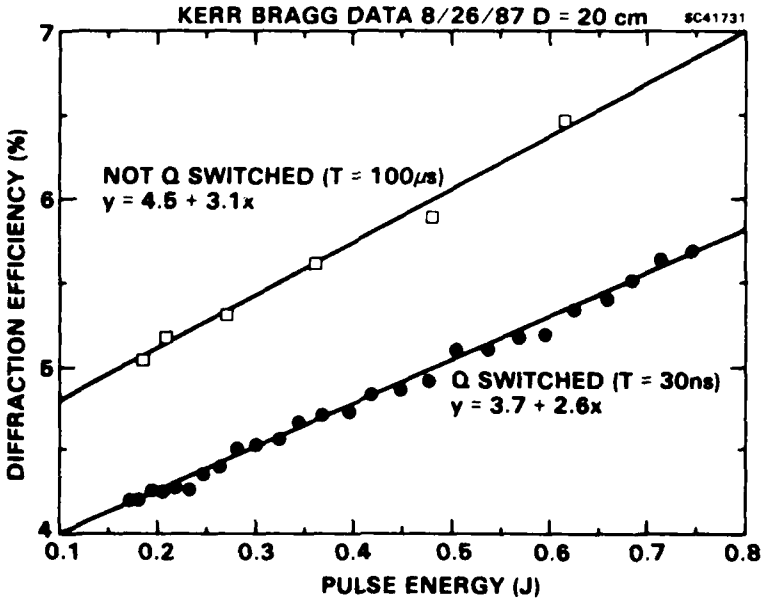

Fig. 14 Experimental data on pulsed laser Kerr-Bragg experiments. Significant increase of diffraction efficiency is observed over less than one order of magnitude increase in the laser pulse energy.

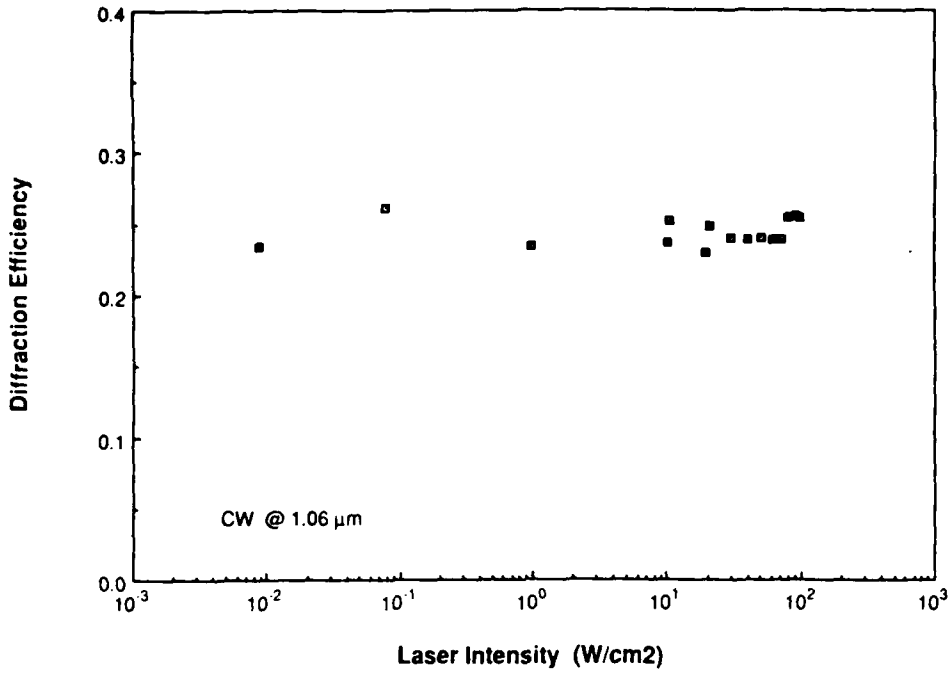

Fig. 15 Acousto-optic diffraction efficiency versus laser power for low power cw laser beam. No significant increase in diffraction efficiency is observed over nearly four orders of magnitude.

trend is understandable in terms of the fact that the acoustic resonances are best excited if the exciting mechanism remains on for times of the order of the phonon lifetimes for the particular acoustic frequency. For comparison, a similar experiment was carried out using a cw laser beam of 1.06 μm wavelength in the same A-O cell. Figure 15 shows that the diffraction efficiency was nearly constant over four orders of magnitude in intensity at these lower intensities ($I \leq 100$ W/cm^2). Clearly, the K-B process is significant only at high laser energies or powers.

2.3 Publications

See list given in Table 2-1.

3.0 APPLICATION CONSIDERATIONS

In this section, we describe the technical background of beam steering techniques and how our studies can address the problem of using nonlinear optical phenomena for agile beam steering of high energy laser beams, and other applications.

3.1 Background

Agile beam steering of laser beams is of interest for a variety of applications, e.g., simple scanning in laser printers, accurate pointing for laser radars, and directed energy weapons for SDI. Figure 16 shows a comparative chart of numerous methods for beam steering. Dashed areas are for performance projections, but actual demonstrations have not been made. Scanning mirrors are the simplest, but they are not suitable in applications where rapid and random access to any resolvable spot is desired. Spinning holograms (also known as "holgons") with spatially varying grating periods are coming into widespread applications in low power laser scanners. They are not shown in the graph in Fig. 16, but in many respects they are similar to rotating mirrors. Acousto-optic devices are essentially zero mass deflectors which use the tuning of acoustic frequencies as a means of controlling deflection angles. Nearly 100% deflection is possible, however, large acoustic powers may be required, particularly when large optical apertures (required for high resolution beam steering) are used.

The primary parameters of interest for beam steering devices are the number of resolvable spots N, and the access time. For A-O devices, the efficiency of beam deflection is also a major performance parameter. The maximum steering angle $\Delta\phi$ is important for determining the resolution (N); however, $\Delta\phi$ by itself is not very important since it can be changed by passive optics, e.g., lenses or mirrors. The resolvable number of spots are determined by the relation

$$N = \Delta\phi/\Delta\beta \quad , \tag{64}$$

where $\Delta\beta$ is the diffraction angle of the optical beam. For A-O devices, it can be shown that

$$N = \Delta f \; T \quad , \tag{65}$$

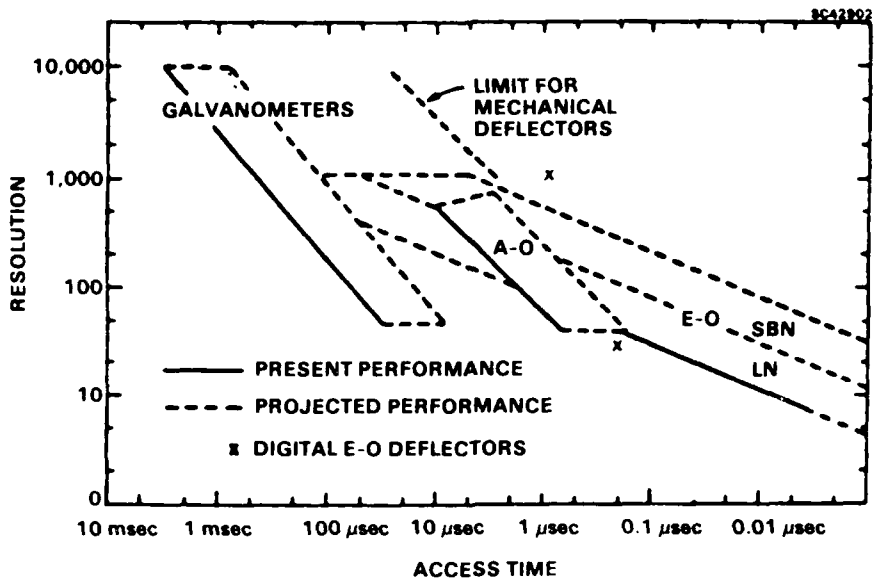

Fig. 16 Comparative chart of various beam steering devices in terms of the resolution (resolvable number of spots) versus the access time. Dashed lines indicate projected, not actual, performance.

where Δf is the frequency bandwidth of the device, and T is the transit time of the acoustic beam across the optical aperture. It is clear that T is also the access time required to switch the beam deflection angle. Acousto-optic devices are interesting in that they are able to address several spots simultaneously, i.e., split the energy of the input beam among several desired directions. This can be accomplished by applying simultaneously several different frequencies of rf signals of various powers to the acoustic transducer.

Use of A-O beam steering devices for SDI applications is very desirable in terms of the generic device capabilities. However, using the conventional A-O devices is quite impractical, because of the high pulse energies, large aperture requirements, and the impracticality of maintaining a uniform and high power acoustic beam across the aperture. In addition, the requirements for the acoustic powers and removal of the resultant heating in the material are quite severe. The Kerr-Bragg process, as we described earlier, is only triggered by acousto-optical events. The actual beam steering is via nondegenerate two-wave mixing between the primary input beam and its (weakly) deflected portion from the acoustic seed beam. Nonlinear optical gratings which are produced are subsequently amplified by light interference and coupling of the nonlinearity to the acoustic phonons. This unique process allows the use of the basic A-O processes for agile beam steering of high

energy beams, without the requirements for supplying large acoustic powers over large apertures. It is then possible to have the important advantages of A-O beam steering for SDI directed energy efforts. These advantages include:

* High efficiency deflection (~ 100%) for high optical energies
* Large resolvable number of spots (N > 1000 for large apertures)
* Fast access times (~ μs/mm aperture)
* Random access
* Simultaneous access to multiple spots (the nonlinear processes require special configurations to implement this aspect of the A-O effects).

Similar arguments can also be given for nondegenerate two-wave mixing effects. These "artificial" photorefractive effects can also be used for beam steering applications, as we briefly describe in the following subsections.

3.2 Kerr-Bragg Beam Steering and Other Applications

The general processes involved in the Kerr-Bragg concept have potential applications as beam steering concepts. As described in Sect. 2, considerable progress has been made in the theoretical and experimental understanding of the stimulated nonlinear effects behind the NDTWM and the related K-B processes. One important question that needs to be answered is whether the acoustic wavefronts will indeed avalanche across the optical aperture by nonlinear optical pumping. Figure 17 shows a schematic illustration of what may be expected. Here, the solid lines show the conceptual avalanching to the right as the optical beam propagates through an initially nonuniform acoustic beam profile (diminished acoustic waves are indicated by dashed lines). This is of particular interest for high frequency acoustic waves where the attenuation in the materials is higher, and launching a uniform acoustic wavefront across a large optical aperture becomes difficult. An additional question is regarding the dynamics of this nonlinear pumping over the aperture, as compared with the temporal length of the optical pulse. The important parameter

is the time required for the acoustic spreading. It must be noted that even for greatly diminished acoustic intensities away from the transducer, the number of phonons remaining is still quite large compared with thermal (noise) phonons. Therefore, it is conceivable that efficient nonlinear pumping can generate the acoustic waves nearly simultaneously over the entire aperture, without the need for acoustic propagation over that distance. This, for example, could occur when optical energies are well above threshold values. There are other important considerations which must be taken into account in terms of competing nonlinear effects. We have begun to analyze some of these effects, such as self-focusing. Such subjects require further theoretical and experimental studies and will be carried out during the proposed follow-on effort.

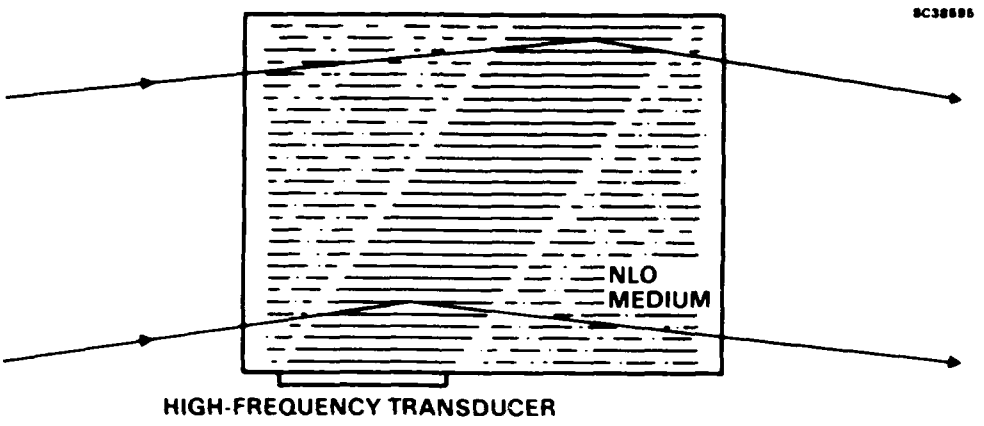

Fig. 17 Conceptual diagram of the Kerr-Bragg process at high acoustic frequencies. Dashed lines indicate decaying acoustic energies. Acoustic spreading over the optical aperture is assisted by nonlinear effects.

The K-B concept can also be used to produce a phase-locked array of high energy laser beams by correcting for dc phase shifts that may be present among the beams. The phase correction can be introduced by applying the phase differences to the acoustic beams through the rf supplied to the transducers, as shown in Fig. 18. In the continuation effort, we will examine such applications of the concepts, in addition to the baseline (primary) effort on the beam steering aspects.

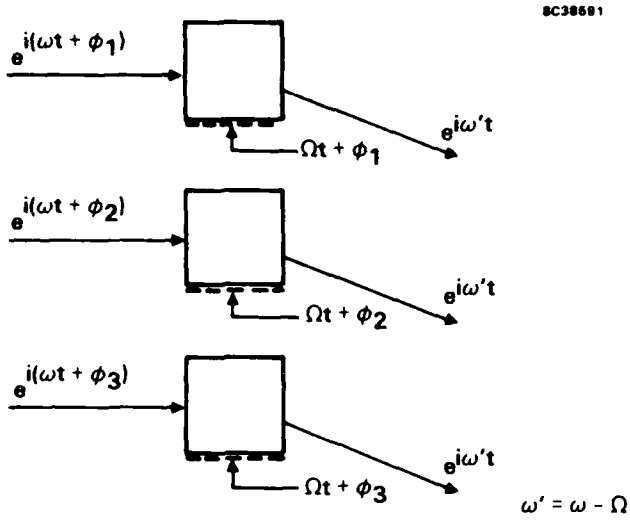

Fig. 18

Conceptual diagram of using the Kerr-Bragg process for a phased optical array.

3.3 Resonant Nondegenerate Two-Wave Mixing in Kerr Media

We will continue to investigate theoretically and experimentally, NDTWM for beam steering applications. The reason for our continued interest is that this process will become competitive with the K-B process, or even advantageous, if the laser energies are very high and the optical apertures are large. Moreover, if it is found that acoustic avalanching across the aperture by nonlinear pumping takes too long compared with the length of the pulse, NDTWM will be the preferred approach. Figure 19 shows the general approach for this concept. The frequency shifted seed beam can be a small beam which is spatially filtered, expanded (now shown in the figure), and subsequently injected into the NDTWM nonlinear medium. Clearly, the frequency shifted seed beam has to be injected into the cell at the proper angle to allow exact wave vector matching. This matching is expected to be an exacting requirement.

The actual geometry for using NDTWM in beam steering can be substantially different than that shown in Fig. 19. Figure 20 shows one concept using 2-D array of transducers sending acoustic waves into a nonlinear medium. A transparent layer of an acoustic reflector provides a receding acoustic wavefront from which initially K-B, and further into the nonlinear medium, NDTWM can take place. The unit cell shown in Fig. 20 can be used to build up a 2-D phased array of nonlinear beam deflectors.

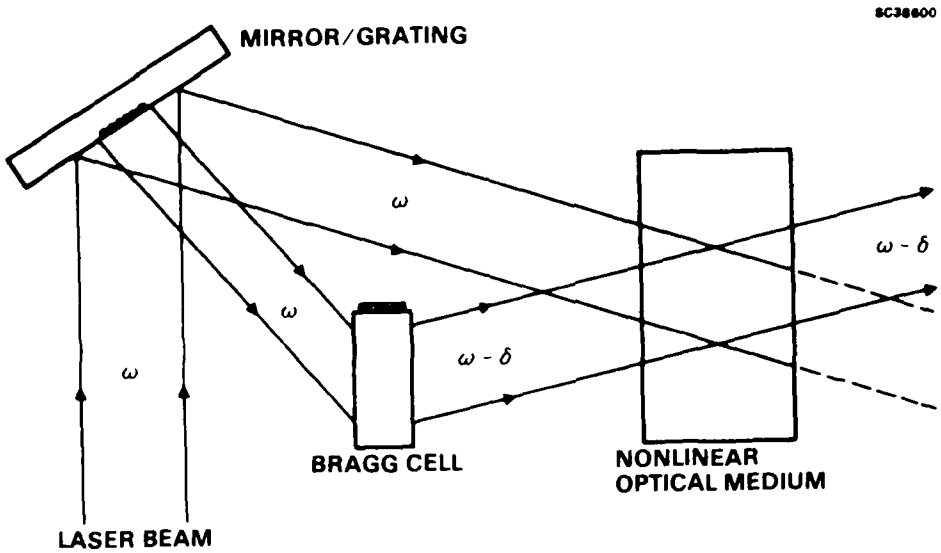

Fig. 19 Schematic diagram of the nondegenerate two-wave mixing setup for beam steering experiments.

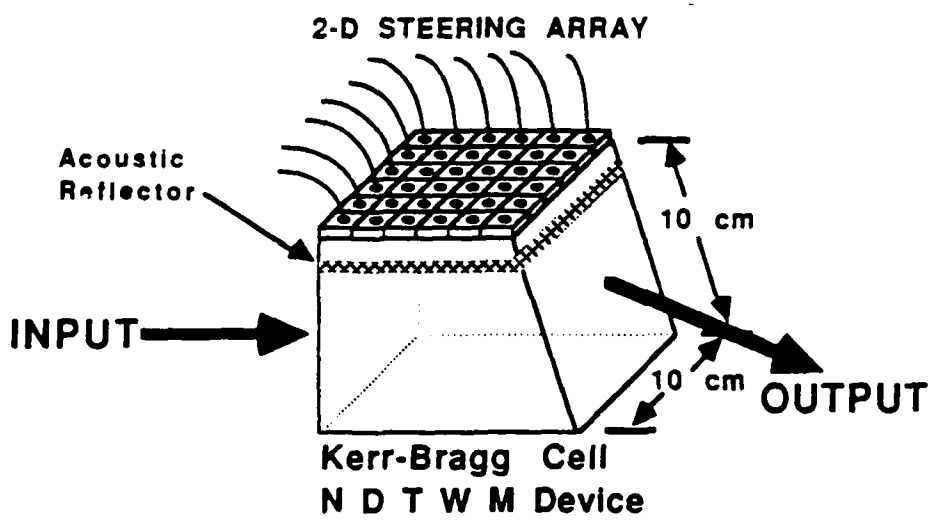

Fig. 20 Schematic diagram of a high frequency, fast access Kerr-Bragg/NDTWM beam steering module.

The NDTWM process can be made spatially resonant to great advantage, if the optical aperture is large enough so that the acoustic waves created at one point on the aperture propagate and increase efficiency at some other point on the aperture. This resonant NDTWM process will be investigated theoretically, and studied in our proposed high energy laser experiments at KMS Fusion.

4.0 REFERENCES

1. J.P. Huignard and A. Marrakchi, "Coherent Signal Beam Amplification in Two-Wave Mixing Experiments with Photorefractive B.S.O. Crystals," Opt. Commun. 38, 249 (1981).

2. J.P. Huignard and A. Marrakchi, "Two-Wave Mixing and Energy Transfer in B.S.O. Crystals: Amplification and Vibration Analysis," Opt. Lett. 622 (1981).

3. R. Fischer, M. Cronin-Golomb, J.O. White and A. Yariv, "Amplified Reflection, Transmission and Self-Oscillation in Real-Time Holography," Opt. Lett. 6, 519 (1981).

4. J.O. White, M. Cronin-Golomb, B. Fischer and A. Yariv, "Coherent Oscillation by Self-Induced Gratings in Photorefractive Crystals," Appl. Phys. Lett. 40, 450-452 (1982).

5. P. Yeh, "Photorefractive Coupling in Ring Resonators," Applied Optics, 23, 2974 (1984).

6. M. Khoshnevisan and P. Yeh, "Nonlinear Optical Doppler Imaging Amplifier," Science Center Patent Disclosure #84SC57.

7. M. Khoshnevisan, P. Yeh and M. Ewbank, "Flexible Rejection Filters," Science Center Patent Disclosure.

8. P. Yeh, "Contra-Directional Two-Wave Mixing in Photorefractive Media," Opt. Comm. 45, 323 (1983).

9. A.E.T. Chiou and P. Yeh, "Beam Cleanup Using Photorefractive Two-Wave Mixing," Opt. Lett. 10, 621 (1985).

10. M. Khoshnevisan and P. Yeh, "Kerr-Bragg Agile Beam Steering Device," Science Center Patent Disclosure, Docket #86SC3 (1986).

11. S.A. Akhmanov, A.P. Sukhorukhov and R.V. Khokhlov, Us. Fiz. Nauk 93, 19 (1967); Sov. Phys. Usp. 93, 609 (1968).

12. N. Bloembergen, Nonlinear Optics (Benjamin, NY, 1965).

13. F. Shimizu and E. Courtens, "Fundamental and Applied Laser Physics," Eds., M.S. Feld, A. Javan and N.A. Kurmit (Wiley, NY, 1971).

14. J. Comly, E. Garmire, J.P. Laussade and A. Yariv, Appl. Phys. 13, 176 (1968).

15. G.A. Askaryan, Soviet Phys. JETP (trans.) 15, 1088 (1962).

16. P.L. Kelley, Phys. REv. Lett. 15, 1088 (1962).

17. V.I. Talanov, Radio Phys. (trans.) 1, 254 (1964).

18. A. Yariv and P. Yeh, Opt. Comm. 27, 295-298 (1978).

19. D.L. Staebler and J.J. Amodei, "Coupled Wave Analysis of Holographic Storage in $LiNbO_3$," J. Appl. Phys. 34, 1042 (1972).

20. V.L. Vinetskii, N.V. Kukhtarev, S.G. Odulov and M.S. Soskin, "Dynamic Self-Diffraction of Coherent Light Beams," Sov. Phys. Usp. 22, 742 (1979).

21. N.V. Kukhtarev, V.B. Markov, S.G. Odulov, M.S. Soskin and V.L. Vinetskii, "Holographic Storage in Electro-Optic Crystals. Beam Coupling and Light Amplification," Ferroelectrics 22, 961 (1979).

22. Y.H. Ja, "Energy Transfer Between Two Beams in Writing a Reflection Volume Hologram in a Dynamic Medium," Opt. Quant. Electron. 14, 547 (1982).

23. P. Yeh, "Electromagnetic Propagation in a Photorefractive Layered Medium," J. Opt. Soc. Am. 73, 1268 (1983).

24. See, for example, A. Yariv and P. Yeh, "Optical Waves in Crystals," page 8 (Wiley, NY, 1984).

25. Tai Chi Wang and P. Yeh, "Codirectional Stimulated Brillouin Scattering," (unpublished).

26. John Reintjes, et al, SDIO/DEO Workship on Nonlinear Optical Techniques for SDI Applications, Kirtland AFB, NM (Oct. 1986).

27. P. Yeh and A.E.T. Chiou, Technical Digest, FG1, CLEO '85, Baltimore, MD (May 1983).

28. V.I. Bespalov, A.A. Betin and G.A. Pasmanik, Izv. Vyssh. Uchebn. Zaved. Radiofiz 21, 961 (1978).

29. J. Goldhar and J.R. Murray, IEEE J. Quantum Electron QE-18, 399 (1982).

30. R.S.F. Chang and N. Djeu, Opt. Lett. 8, 139 (1983).

31. R.S.F. Chang et al, Technical Digest, WA2, CLEO '85, Baltimore, MD (May 1985).

32. J. Fienberg, Opt. Lett. 7, 486 (1982).

33. A.E.T. Chiou and P. Yeh, Technical Digest, ThG1, OSA 1985 Annual Meeting, Washington, D.C. (Oct. 1985).

34. R.W. Dixon, J. Appl. Phys. 38, 5149 (1967).

35. See, for example, W. Kaiser and M. Maier, "Stimulated Rayleigh, Brillouin and Raman Spectroscopy," Chapter E2 of Laser Handbook, edited F.T. Arecchi and E.O. Schulz-DuBois (North-Holland Publ. Co. 1972).

36. B.Y. Zeldovich, V.V. Popovichev, V.V. Ragulskii and F.S. Faisullov, Sov. Phys. JETP Lett. 15, 109 (1972).

37. M. Maier, Phys. Rev. 166, 113 (1968).

38. See, for example, A. Yariv, "Quantum Electronics," 2nd Ed. p. 492, J. Wiley (1975).

39. See, for example, A. Yariv, and P. Yeh, "Optical Waves in Crystals," Chapters 9-11, J. Wiley (1983).

40. D.A. Pinnow, "Elastooptical Materials," pp. 478-488, CRC Handbook of Lasers, Chemical Rubber Co. (1971).

41. T.Y. Chang, Opt. Eng. 20, 220 (1981).

42. See, for example, A. Yariv and P. Yeh, "Optical Waves in Crystals," (Wiley, 1984), chapter 9.

43. P. Yeh, J. Opt. Soc. Am. B3, 747 (1986).

44. A. Korpel, R. Adler and B. Alpiner, Appl. Phys. Lett. 5, 86 (1964).

45. F. Aronowitz and R.J. Collins, Appl. Phys. Lett. 9, 55 (1966).

46. P. Yeh and M. Khoshnevisan, SPIE 487, 102 (1984).

APPENDIX A

The solution of the nonlinear coupled differential Eqs. (12) and (13) is derived in this appendix.

By adding the two equations in (12) and carrying out the integration we obtain

$$I_1 + I_2 = C \exp(-\alpha z) \tag{A.1}$$

where C is a constant equal to $I_1(o) + I_2(o)$. Using Eqs. (A.1) and (12), we can eliminate I_2 and obtain

$$\frac{d}{dz} I_1 + (\alpha + gC\, e^{-\alpha z})\, I_1 = g I_1^2 \tag{A.2}$$

which is a Bernoulli equation and can be integrated directly. The solution is

$$I_1(z)^{-1} = e^{\int P(z)dz} \{-g \int e^{-\int P(z)dz} + C'\} \tag{A.3}$$

where C' is a constant of integration and P(z) is given by

$$P(z) = \alpha + gC\, e^{-\alpha z} \quad . \tag{A.4}$$

To simplify Eq. (A.3), we need to use the following integral formula

$$\int e^{-ax+be^{-ax}}\, dx = -\frac{1}{ab}\, e^{be^{-ax}} \quad . \tag{A.5}$$

Using Eqs. (A.4) and (A.5), Eq. (A.3) can be written

$$I_1(z) = \frac{C\, e^{-\alpha z}}{1 + CC' \exp[-\frac{1}{\alpha} gC \exp(-\alpha z)]} \quad . \tag{A.6}$$

Putting z = 0 in Eq. (A.6) and solving for C', we obtain

$$C' = \frac{1}{C} \frac{I_2(o)}{I_1(o)} \exp[\frac{1}{\alpha} gC] \tag{A.7}$$

where we recall that $C = I_1(o) + I_2(o)$. Using the definitions for m and γ from Eqs. (18) and (19), respectively, and Eq. (A.7), $I_1(z)$ can be rewritten in the form of Eq. (16). The solution for $I_2(z)$ can be obtained from Eqs. (16) and (A.1). This completes the solution for $I_1(z)$ and $I_2(z)$.

Solution for the phase ψ_1 and ψ_2 can be obtained by substituting Eqs. (16) and (17) for $I_1(z)$ and $I_2(z)$, respectively, into Eq. (13) and carrying out the integration. The process requires the following integral formula:

$$\int \frac{e^{-\alpha x}}{1 + B \exp[\frac{1}{\alpha} A \exp(-\alpha x)]} \, dx = \frac{1}{A} \log \{1 + \frac{1}{B} \exp[-\frac{1}{\alpha} A \exp(-\alpha x)]\} \quad . \tag{A.8}$$

Using the expressions for $I_1(z)$ and $I_2(z)$ and the above formula, we arrive at Eqs. (20) and (21). This completes the derivation of $\psi_1(z)$ and $\psi_2(z)$.

APPENDIX B
ELECTROSTRICTIVE AND PHOTOELASTIC EFFECTS

We begin by examining the components T_{ij} of the stress tensor T, as related to the generalized strain components S_{ij} of the strain tensor S. Generalizing from Eq. (26), we can write the electrostrictive stress as

$$T_{ij} = -\frac{1}{2}\,\gamma_{ijk\ell}\,E_k E_\ell \quad , \tag{B.1}$$

where E_i are the components of the electric field. From thermodynamics,

$$T_{ij} = -\left(\frac{\partial U}{\partial S_{ij}}\right) = \frac{\partial}{\partial S_{ij}}\left(\frac{1}{2}\,D_k\,\frac{1}{\epsilon_{k\ell}}\,D_\ell\right)$$

$$= -\frac{\partial}{\partial S_{ij}}\left[\frac{1}{2\epsilon_o}\,D_k\,\left(\frac{1}{n^2}\right)_{k\ell}\,D_\ell\right]$$

$$= -\frac{1}{2\epsilon_o}\left[\frac{\partial}{\partial S_{ij}}\left(\frac{1}{n^2}\right)_{k\ell}\right] D_k D_\ell$$

$$= -\frac{1}{2\epsilon_o}\left[p_{ijk\ell}\right]\,\epsilon_k\epsilon_\ell E_k E_\ell \quad . \tag{B.2}$$

Therefore,

$$\gamma_{ijk\ell} = \epsilon_0\, n^2_k\, n^2_\ell\, p_{k\ell ij} \quad . \tag{B.3}$$

APPENDIX C

The solution of the nonlinear coupled Eqs. (56) is derived in this appendix.

By adding the two equations in Eqs. (56) and carrying out the integration, we obtain

$$I_1 + I_2 = c, \tag{C.1}$$

where c is a constant equal to the incident intensity I at z = 0.

Let $I_2 = y$ and $I_1 = c - y$, the second of Eqs. (56) becomes

$$y' = gy\ (c - y) + 2\kappa\sqrt{(c - y)y} \tag{C.2}$$

To integrate this equation, we further let

$$y = c \sin^2 u. \tag{C.3}$$

Substitution of Eq. (C.3) for y into Eq. (C.2) leads to

$$\frac{2du}{1 + b \sin 2u} = 2\kappa dz \tag{C.4}$$

where

$$b = \frac{gc}{4\kappa} = \frac{gI}{4\kappa} \tag{C.5}$$

Equation (C.4) can now be integrated and the result is

$$\frac{2}{\sqrt{1-b^2}} \tan^{-1} \frac{\tan u + b}{\sqrt{1-b^2}} = .2\kappa z + \text{constant} \qquad \text{(C.6)}$$

Here, we note that the result in Eq. (C.6) is also valid for $|b| > 1$. The constant of integration is determined by the boundary condition at $z = 0$. Using $u = 0$ at $z = 0$, we obtain

$$\frac{2}{\sqrt{1-b^2}} \tan^{-1} \frac{\tan u + b}{\sqrt{1-b^2}} = 2\kappa z + \frac{2}{\sqrt{1-b^2}} \tan^{-1} \frac{b}{\sqrt{1-b^2}} \qquad \text{(C.7)}$$

Equation (58) can now be obtain directly from Eq. (C.7) after a few steps of elementary trigonometry.

END
DATED
FILM
8-88
DTIC